

# Meson loop effects in the NJL model at zero and non-zero temperature

M. Oertel, M. Buballa and J. Wambach

*Institut für Kernphysik, TU Darmstadt,*

*Schlossgartenstr. 9, 64289 Darmstadt, Germany*

## Abstract

We compare two different possibilities to include meson-loop corrections in the Nambu–Jona-Lasinio model: a strict  $1/N_c$ -expansion in next-to-leading order and a non-perturbative scheme corresponding to a one-meson-loop approximation to the effective action. Both schemes are consistent with chiral symmetry, in particular with the Goldstone theorem and the Gell-Mann–Oakes–Renner relation. The numerical part at zero temperature focuses on the pion and the  $\rho$ -meson sector. For the latter the meson-loop-corrections are crucial in order to include the dominant  $\rho \rightarrow \pi\pi$ -decay channel, while the standard Hartree + RPA approximation only contains unphysical  $q\bar{q}$ -decay channels. We find that  $m_\pi, f_\pi, \langle \bar{\psi}\psi \rangle$  and quantities related to the  $\rho$ -meson self-energy can be described reasonably with one parameter set in the  $1/N_c$ -expansion scheme, whereas we did not succeed to obtain such a fit in the non-perturbative scheme. We also investigate the temperature dependence of the quark condensate. Here we find consistency with chiral perturbation theory to lowest order. Similarities and differences of both schemes are discussed.

# 1 Introduction

During the last few years one of the principal goals in nuclear physics has been to explore the phase structure of QCD. Along with this comes the investigation of hadron properties in the vacuum as well as in hot or dense matter. In principle, all properties of strongly interacting particles should be derived from QCD. However, at least in the low-energy regime, where perturbation theory is not applicable, this is presently limited to a rather small number of observables which can be studied on the lattice, while more complex processes can either be addressed by chiral perturbation theory or within effective model calculations which try to incorporate the relevant degrees of freedom.

So far the best descriptions of hadronic spectra, decays and scattering processes are obtained within phenomenological hadronic models. For instance the pion electromagnetic form factor in the time-like region can be reproduced rather well within a simple vector dominance model with a dressed  $\rho$ -meson which is constructed by coupling a bare  $\rho$ -meson to a two-pion intermediate state [1, 2]. Models of this type have been successfully extended to investigate medium modifications of vector mesons and to calculate dilepton production rates in hot and dense hadronic matter [3].

In this situation one might ask how the phenomenologically successful hadronic models emerge from the underlying quark structure and the symmetry properties of QCD. Since this question cannot be answered at present from first principles it has to be addressed within quark models. For light hadrons chiral symmetry and its spontaneous breaking in the physical vacuum through instantons plays the decisive role in describing the two-point correlators [4] with confinement being much less important. This feature is captured by the Nambu–Jona-Lasinio (NJL) model in which the four-fermion interactions can be viewed as being induced by instantons. Furthermore the model allows a study of the chiral phase transition as well as the examination of the influence of (partial) chiral symmetry restoration on the properties of light hadrons.

The study of hadrons within the NJL model has of course a long history. In fact, mesons of various quantum numbers have already been discussed in the original papers by Nambu and Jona-Lasinio [5] and by many authors thereafter (for reviews see [6, 7, 8]).

In most of these works quark masses are calculated in mean-field approximation (Hartree or Hartree-Fock) while mesons are constructed as correlated quark-antiquark states (RPA). This corresponds to a leading-order approximation in  $1/N_c$ , the inverse number of colors. With the appropriate choice of parameters chiral symmetry, which is an (approximate) symmetry of the model Lagrangian, is spontaneously broken in the vacuum and pions emerge as (nearly) massless Goldstone bosons. While this is clearly one of the successes of the model, the description of other mesons is more problematic. One reason is the fact that the NJL model does not confine quarks. As a consequence a meson can decay into free constituent quarks if its mass is larger than twice the constituent quark mass  $m$ . Hence, for a typical value of  $m \sim 300$  MeV, the  $\rho$ -meson with a mass of 770 MeV, for instance, would be unstable against decay into quarks. On the other hand the physical decay channel of the  $\rho$ -meson into two pions is not included in the standard approximation. Hence, even if a large constituent quark mass is chosen in order to suppress the unphysical decays into quarks, one obtains a poor description of the  $\rho$ -meson propagator and related observables, like the pion electromagnetic form factor.

Similar problems arise if one wants to study the phase structure of strongly interacting matter within a mean-field calculation for the NJL model, although this has been done by many authors (see e.g. [7, 8, 9, 10]). In these calculations the thermodynamics is entirely driven by unphysical unconfined quarks even at low temperatures and densities, whereas the physical degrees of freedom, in particular the pion, are missing.

This and other reasons have motivated several authors to go beyond the standard approximation scheme and to include mesonic fluctuations. In Ref. [11] a quark-antiquark  $\rho$ -meson is coupled via a quark triangle to a two-pion state. Also higher-order corrections to the quark self-energy [12] and to the quark condensate [13] have been investigated. However, as the most important feature of the NJL model is chiral symmetry, one should use an approximation scheme which conserves the symmetry properties, to ensure the existence of massless Goldstone bosons.

A non-perturbative symmetry conserving approximation scheme has been discussed in Refs. [14] and [15]. In Ref. [14] a correction term to the quark self-energy is included in the gap equation. The authors find a consistent scheme to describe mesons and show the validity of the Goldstone theorem and the Goldberger-Treiman relation in that scheme. The authors of Ref. [15] use a one-meson-loop approximation to the effective action in a bosonized NJL model. The structure of the meson propagators turns out to be the same as in the approach of Ref. [14]. Based on this scheme various authors have investigated the effect of meson-loop corrections on the pion electromagnetic form factor [16] and on  $\pi$ - $\pi$  scattering in the vector [17] and the scalar channel [18]. However, since the numerical evaluation of the multi-loop diagrams is rather involved, in these references the exact expressions are approximated by low-momentum expansions.

Another possibility to construct a symmetry conserving approximation scheme beyond Hartree approximation and RPA is a strict  $1/N_c$ -expansion up to next-to-leading order. Whereas in the approximation scheme mentioned above the gap equation is modified in a selfconsistent way, the corrections in the  $1/N_c$ -expansion scheme are perturbative. The consistency of the  $1/N_c$ -expansion scheme with chiral symmetry has already been shown in Ref. [14]. It has been studied in more detail in Refs. [19, 20]. Recently such an expansion has been discussed also in the framework of a non-local generalization of the NJL model [21].

In the present paper we compare the results obtained in the non-perturbative scheme with those obtained in the  $1/N_c$ -expansion scheme. In vacuum we focus our discussion on the pion and the  $\rho$ -meson, calculated with the full momentum dependence of all expressions. Within the  $1/N_c$ -expansion scheme the influence of mesonic fluctuations on the pion propagator has been examined closely in Ref. [19]. This was mainly motivated by recent works by Kleinert and Van den Bossche [22], who claim that chiral symmetry is *not* spontaneously broken in the NJL model as a result of strong mesonic fluctuations. In Ref. [19] we argue that because of the non-renormalizability of the NJL model new divergences and hence new cutoff parameters emerge if one includes meson loops. Following Refs. [14] and [15] we regularize the meson loops by an independent cutoff parameter  $\Lambda_M$ . The results are, of course, strongly dependent on this parameter. Whereas for moderate values of  $\Lambda_M$  the pion properties change only quantitatively, strong instabilities are encountered for larger values of  $\Lambda_M$ . In Ref. [19] we suggested that this might be a hint for an instability of the spontaneously broken vacuum state. It turns out that the

same type of instabilities also emerge in the non-perturbative scheme. This allows for an analysis of the vacuum structure and therefore for a more decisive answer to the question whether chiral symmetry gets indeed restored due to strong mesonic fluctuations within this approximation.

In any case, in the  $1/N_c$ -expansion scheme the region of parameter values where instabilities emerge in the pion propagator is far away from a realistic parameter set [20]. We used  $m_\pi, f_\pi, \langle \bar{\psi}\psi \rangle$  and the  $\rho$ -meson spectral function to fix the parameters. The last one is particularly suited, as it cannot be described realistically without taking into account pion loops, to fix the parameters. An important result of the analysis in Ref. [20] was that such a fit can be achieved with a constituent quark mass which is large enough such that the unphysical  $q\bar{q}$ -threshold opens above the  $\rho$ -meson peak. Since the constituent quark mass is not an independent input parameter this was not clear a priori. In this paper we will try the same for the selfconsistent scheme. It turns out that it is not possible to find a parameter set, where the constituent quark mass comes out large enough to describe the properties of the  $\rho$ -meson reasonably. In fact we encounter instabilities in the  $\rho$ -meson propagator which are similar to those we found in the pion propagator for large  $\Lambda_M$ .

The inclusion of meson loop effects should also improve the thermodynamics of the model considerably. A first insight on the influence of mesonic fluctuations upon the thermodynamics can be obtained via the temperature dependence of the quark condensate. It has been shown in Ref. [23] that in the selfconsistent scheme the low-temperature behavior is dominated by pionic degrees of freedom which is a considerable improvement on calculations in Hartree approximation where quarks are the only degrees of freedom. Within this scheme the lowest-order chiral perturbation theory result can be reproduced. This is also the case for the  $1/N_c$ -expansion scheme which will be demonstrated in the last part of this paper. The non-perturbative scheme also allows for an examination of the chiral phase transition [23], whereas this is not possible within the  $1/N_c$ -expansion scheme.

The paper is organized as follows. In Sec. 2 we begin with a brief summary of the standard approximation scheme used in the NJL model to describe quarks and mesons and afterwards present the scheme for describing quantities in next-to-leading order in  $1/N_c$ . In Sec. 3 we discuss the non-perturbative approximation scheme. The consistency of these schemes with the Goldstone theorem and with the Gell-Mann Oakes Renner relation will be shown in Sec. 4. The numerical results at zero temperature will be presented in Sec. 5. The temperature dependence of the quark condensate at non-zero temperature within the two above mentioned approximation schemes will be studied in Sec. 6. Finally, conclusions are drawn in Sec. 7.

## 2 The NJL model in leading order and next-to-leading order in $1/N_c$

### 2.1 The standard approximation scheme: Hartree + RPA

We consider the following generalized NJL-model Lagrangian:

$$\mathcal{L} = \bar{\psi}(i\cancel{\partial} - m_0)\psi + g_s [(\bar{\psi}\psi)^2 + (\bar{\psi}i\gamma_5\vec{\tau}\psi)^2] - g_v [(\bar{\psi}\gamma^\mu\vec{\tau}\psi)^2 + (\bar{\psi}\gamma^\mu\gamma_5\vec{\tau}\psi)^2], \quad (2.1)$$

where  $\psi$  is a quark field with  $N_f = 2$  flavors and  $N_c = 3$  colors.  $g_s$  and  $g_v$  are coupling constants with dimension  $length^2$ . In contrast to QCD, color is not related to a gauge symmetry in this model, but only relates to a counting of degrees of freedom. However, if one defines the coupling constants to be of the order  $1/N_c$ , the large- $N_c$  behavior of the model agrees with that of QCD [14, 15]. Although we are not interested in the behavior of the model for arbitrary numbers of colors in the present article, the  $1/N_c$ -expansion is introduced for the purpose of book-keeping. This will allow us to take into account mesonic fluctuations in a symmetry conserving way. In order to establish the expansion scheme, the number of colors will be formally treated as variable. All numerical calculations will be performed, however, with the physical value,  $N_c = 3$ .

In the limit of vanishing current quark masses  $m_0$  (“chiral limit”) the above Lagrangian is invariant under global  $SU(2)_L \times SU(2)_R$  transformations. For a sufficiently large scalar attraction this symmetry is spontaneously broken. This has mostly been studied within the (Bogoliubov-) Hartree approximation.\*

The Dyson equation for the quark propagator in Hartree approximation is diagrammatically shown in Fig. 1. The selfconsistent solution of this equation leads to a momentum independent quark self-energy  $\Sigma_H$  and therefore only gives a correction to the quark mass:

$$m = m_0 + \Sigma_H(m) = m_0 + \sum_M 2ig_M \int \frac{d^4p}{(2\pi)^4} \text{Tr} [\Gamma_M S(p)]. \quad (2.2)$$

Usually,  $m$  is called the “constituent quark mass”. Here  $S(p) = (\cancel{p} - m)^{-1}$  is the (Hartree) quark propagator and “Tr” denotes a trace in color, flavor and Dirac space. The sum runs over all interaction channels  $M = \sigma, \pi, \rho, a_1$  with  $\Gamma_\sigma = \mathbb{1}$ ,  $\Gamma_\pi^a = i\gamma_5\tau^a$ ,  $\Gamma_\rho^{\mu a} = \gamma^\mu\tau^a$  and  $\Gamma_{a_1}^{\mu a} = \gamma^\mu\gamma_5\tau^a$ . The corresponding coupling constants are  $g_M = g_s$  for  $M = \sigma$  or

---

\* Because of the local 4-fermion interaction in the Lagrangian, exchange diagrams can always be cast in the form of direct diagrams via a Fierz transformation. This is well known from zero-range interactions in nuclear physics. In particular the Hartree-Fock approximation is equivalent to the Hartree approximation with appropriately redefined coupling constants. In this sense we call the Hartree approximation the “standard approximation” to the NJL model, although in several references a Hartree-Fock approximation has been performed.



Figure 1: The Dyson equation for the quark propagator in the Hartree approximation (solid lines). The dashed lines denote the bare quark propagator.

$M = \pi$  and  $g_M = g_v$  for  $M = \rho$  or  $M = a_1$ . Of course, only the scalar channel ( $M = \sigma$ ) contributes in vacuum. One gets

$$m = m_0 + 2ig_s 4N_c N_f \int \frac{d^4 p}{(2\pi)^4} \frac{m}{p^2 - m^2 + i\epsilon}. \quad (2.3)$$

In a  $1/N_c$  expansion of the quark self-energy the Hartree approximation corresponds to the leading order. Since  $g_s$  is of the order  $1/N_c$  the constituent quark mass  $m$ , and hence the quark propagator are of the order unity.

For sufficiently large couplings  $g_s$  Eq. (2.3) allows for a finite constituent quark mass  $m$  even in the chiral limit. In the mean-field approximation this solution minimizes the ground state energy. Because of the related gap in the quark spectrum, one usually refers to this equation as the gap equation, in analogy to BCS theory.

A closely related quantity is the quark condensate, which is generally given by

$$\langle \bar{\psi}\psi \rangle = -i \int \frac{d^4 p}{(2\pi)^4} \text{Tr} S(p). \quad (2.4)$$

In Hartree approximation one immediately gets from the gap equation

$$\langle \bar{\psi}\psi \rangle^{(0)} = -\frac{m - m_0}{2g_s}, \quad (2.5)$$

where we have used the superscript (0) to indicate that this corresponds to a Hartree approximation.

Mesons are described via a Bethe-Salpeter equation. Here the leading order in  $1/N_c$  is given by a random phase approximation (RPA) without Pauli-exchange diagrams. This is diagrammatically shown in Fig. 2. The elementary building blocks of this scheme are the quark-antiquark polarization functions

$$\Pi_M(q) = -i \int \frac{d^4 p}{(2\pi)^4} \text{Tr} [\Gamma_M iS(p + \frac{q}{2}) \Gamma_M iS(p - \frac{q}{2})], \quad (2.6)$$

with  $\Gamma_M$ ,  $M = \sigma, \pi, \rho, a_1$  as defined above. Again, the trace has to be taken in color, flavor and Dirac space. Iterating the scalar (pseudoscalar) part of the four-fermion interaction one obtains for the sigma meson (pion):

$$D_\sigma(q) = \frac{-2g_s}{1 - 2g_s \Pi_\sigma(q)}, \quad D_\pi^{ab}(q) \equiv D_\pi(q) \delta_{ab} = \frac{-2g_s}{1 - 2g_s \Pi_\pi(q)} \delta_{ab}. \quad (2.7)$$

Here  $a$  and  $b$  are isospin indices and we have used the notation  $\Pi_\pi^{ab}(q) \equiv \Pi_\pi(q) \delta_{ab}$ .

In the vector channel this can be done in a similar way. Using the transverse structure of the polarization loop in the vector channel,

$$\Pi_\rho^{\mu\nu,ab}(q) = \Pi_\rho(q) T^{\mu\nu} \delta_{ab}; \quad T^{\mu\nu} = (-g^{\mu\nu} + \frac{q^\mu q^\nu}{q^2}), \quad (2.8)$$

one obtains for the  $\rho$ -meson

$$D_\rho^{\mu\nu,ab}(q) \equiv D_\rho(q) T^{\mu\nu} \delta_{ab} = \frac{-2g_v}{1 - 2g_v \Pi_\rho(q)} T^{\mu\nu} \delta_{ab}. \quad (2.9)$$

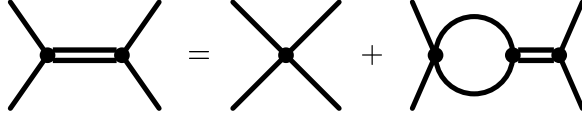


Figure 2: *The Bethe-Salpeter equation for the meson propagator in the RPA (double line). The solid lines indicate quark propagators.*

Analogously, the  $a_1$  can be constructed from the transverse part of the axial polarization function  $\Pi_{a_1}$ . As discussed e.g. in Ref. [24]  $\Pi_{a_1}^{\mu\nu}$  also contains a longitudinal part which contributes to the pion. Although there is no conceptual problem in including this mixing we will neglect it in the present paper in order to keep the structure of the model as simple as possible.

It follows from Eqs. (2.6) - (2.9) that the functions  $D_M(q)$  are of order  $1/N_c$ . Their explicit forms are given in App. B. For simplicity we will call them “propagators”, although strictly speaking, they should be interpreted as the product of a renormalized meson propagator with a squared quark-meson coupling constant. The latter is given by the inverse residue of the function  $D_M(q)$ , while the pole position determines the meson mass:

$$D_M^{-1}(q)|_{q^2=m_M^{2(0)}} = 0, \quad g_{Mqq}^{-2(0)} = \frac{d\Pi_M(q)}{dq^2}|_{q^2=m_M^{2(0)}}. \quad (2.10)$$

Again the superscript (0) indicates that  $m_M^{2(0)}$  and  $g_{Mqq}^{-2(0)}$  are quantities in RPA. One easily verifies that they are of order unity and  $1/\sqrt{N_c}$ , respectively.

## 2.2 Next-to-leading order corrections

With the help of the gap equation, Eq. (2.3), one can show that the “standard scheme”, i.e. Hartree approximation + RPA, is consistent with chiral symmetry. For instance, in the chiral limit pions are massless, as required by the Goldstone theorem. Of course one would like to preserve this feature when one goes beyond the standard scheme. One way to accomplish this is to perform a strict  $1/N_c$  expansion, systematically including higher-order corrections. In this subsection we want to construct the quark self-energy and the mesonic polarization functions in next-to-leading order in  $1/N_c$ .

The correction terms to the quark self-energy,

$$\delta\Sigma(p) = \delta\Sigma^{(a)} + \delta\Sigma^{(b)}(p), \quad (2.11)$$

are shown in Fig. 3. In these diagrams the single lines and the double lines correspond to quark propagators in the Hartree approximation (order unity) and to meson propagators in the RPA (order  $1/N_c$ ), respectively. Recalling that one obtains a factor  $N_c$  for a closed quark loop one finds that both diagrams are of order the  $1/N_c$ . One can also easily convince oneself that there are no other self-energy diagrams of that order.

According to Eq. (2.4), the  $1/N_c$ -correction to the quark condensate is given by

$$\delta\langle\bar{\psi}\psi\rangle = -i \int \frac{d^4p}{(2\pi)^4} \text{Tr} \delta S(p), \quad (2.12)$$

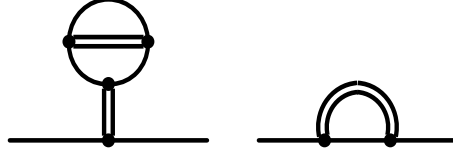


Figure 3: The  $1/N_c$ -corrections  $\delta\Sigma^{(a)}$  (left) and  $\delta\Sigma^{(b)}$  (right) to the quark self-energy.

with

$$\delta S(p) = S(p) \delta\Sigma(p) S(p) \quad (2.13)$$

being the  $1/N_c$ -correction to the Hartree quark propagator  $S(p)$ . Since we are interested in a strict  $1/N_c$  expansion, the self-energy correction must not be iterated.

The  $1/N_c$ -corrected mesonic polarization diagrams read

$$\tilde{\Pi}_M(q) = \Pi_M(q) + \sum_{k=a,b,c,d} \delta\Pi_M^{(k)}(q). \quad (2.14)$$

The four correction terms  $\delta\Pi_M^{(a)}$  to  $\delta\Pi_M^{(d)}$  together with the leading-order term  $\Pi_M$  are shown in Fig. 4. Again, the lines in this figure correspond to Hartree quarks and RPA mesons. Since the correction terms consist of either one RPA propagator and one quark loop or two RPA propagators and two quark loops they are of the order unity, whereas the leading-order term is of the order  $N_c$ .

In analogy to Eqs. (2.7), (2.9) and (2.10) the corrected meson propagators are given by

$$\tilde{D}_M(q) = \frac{-2g_M}{1 - 2g_M\tilde{\Pi}_M(q)}, \quad (2.15)$$

while the corrected meson masses are defined by the pole positions of the propagators:

$$\tilde{D}_M^{-1}(q)|_{q^2=m_M^2} = 0. \quad (2.16)$$

As we will see in Sec. 4.2 this scheme is consistent with the Goldstone theorem, i.e. in the chiral limit it leads to massless pions. Note, however, that because of its implicit definition  $m_M$  contains terms of arbitrary orders in  $1/N_c$ , although we start from a strict expansion of the inverse meson propagator up to next-to-leading order. This will be important in the context of the Gell-Mann–Oakes–Renner relation.

For a more explicit evaluation of the correction terms it is advantageous to introduce the quark triangle and box diagrams which are shown in Fig. 5. The triangle diagrams entering into  $\delta\Sigma^{(a)}$ ,  $\delta\Pi_M^{(a)}$  and  $\delta\Pi_M^{(d)}$  can be interpreted as effective three-meson vertices. For external mesons  $M_1$ ,  $M_2$  and  $M_3$  they are given by

$$-i\Gamma_{M_1,M_2,M_3}(q,p) = -\int \frac{d^4k}{(2\pi)^4} \left\{ \text{Tr} [\Gamma_{M_1} iS(k) \Gamma_{M_2} iS(k-p) \Gamma_{M_3} iS(k+q)] \right. \\ \left. + \text{Tr} [\Gamma_{M_1} iS(k-q) \Gamma_{M_3} iS(k+p) \Gamma_{M_2} iS(k)] \right\} \quad (2.17)$$

with the operators  $\Gamma_M$  as defined below Eq. (2.2). We have summed over both possible orientations of the quark loop. For later convenience we also define the constant



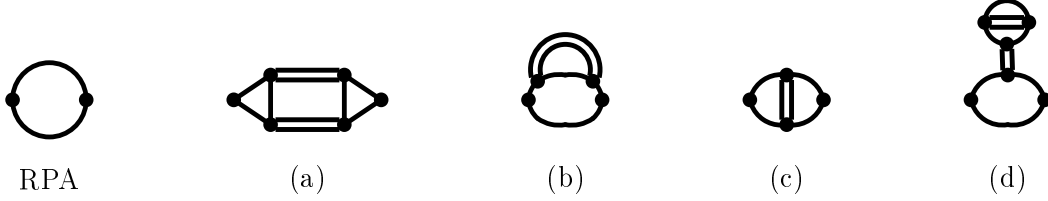


Figure 4: Contributions to the mesonic polarization function in leading (RPA) and next-to-leading order in  $1/N_c$ .

$$\Delta = \frac{1}{2} \int \frac{d^4 p}{(2\pi)^4} \sum_M (-iD_M(p)) (-i\Gamma_{M,M,\sigma}(p, -p)), \quad (2.18)$$

which corresponds to a quark triangle coupled to an external scalar vertex and a closed meson loop.

The quark box diagrams are effective four-meson vertices and are needed for the evaluation of  $\delta\Pi_M^{(b)}$  and  $\delta\Pi_M^{(c)}$ . If one again sums over both orientations of the quark loop they are given by

$$\begin{aligned} & -i\Gamma_{M_1, M_2, M_3, M_4}(p_1, p_2, p_3) \\ &= \int \frac{d^4 k}{(2\pi)^4} \left( \text{Tr} [\Gamma_{M_1} iS(k) \Gamma_{M_2} iS(k - p_2) \Gamma_{M_3} iS(k - p_2 - p_3) \Gamma_{M_4} iS(k + p_1)] \right. \\ & \quad \left. + \text{Tr} [\Gamma_{M_1} iS(k - p_1) \Gamma_{M_4} iS(k + p_2 + p_3) \Gamma_{M_3} iS(k + p_2) \Gamma_{M_2} iS(k)] \right) \end{aligned} \quad (2.19)$$

With these definitions the various diagrams can be written in a relatively compact form. For the momentum independent correction term to the quark self-energy we get

$$\delta\Sigma^{(a)} = -\frac{1}{2} D_\sigma(0) \sum_M \int \frac{d^4 p}{(2\pi)^4} D_M(p) \Gamma_{M,M,\sigma}(p, -p) = D_\sigma(0) \Delta. \quad (2.20)$$

In principle there should be also a sum over the quantum numbers of the meson which connects the quark loop with the external quark legs, but all contributions from other mesons than the  $\sigma$ -meson vanish. The factor of  $1/2$  is a symmetry factor which is needed because otherwise the sum over the two orientations of the quark propagators, which is contained in the definition of the quark triangle vertex (Eq. (2.17)) would lead to double counting.

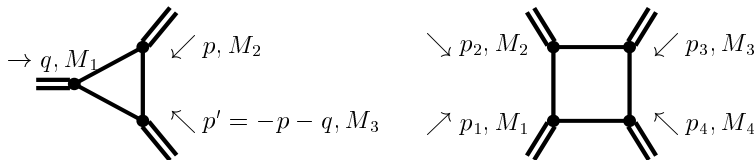


Figure 5: (Left) The quark triangle vertex  $-i\Gamma_{M_1, M_2, M_3}(q, p)$ . (Right) The quark box vertex  $-i\Gamma_{M_1, M_2, M_3, M_4}(p_1, p_2, p_3)$ .

The evaluation of the momentum dependent correction term  $\delta\Sigma^{(b)}$  is straight forward:

$$\delta\Sigma^{(b)}(k) = i \sum_M \int \frac{d^4p}{(2\pi)^4} D_M(p) \Gamma_M S(k-p) \Gamma_M . \quad (2.21)$$

Inserting these expressions for  $\delta\Sigma^{(a)}$  and  $\delta\Sigma^{(b)}$  into Eq. (2.13), the  $1/N_c$ -correction term to the quark condensate, Eq. (2.12), can be brought into the form

$$\delta\langle\bar{\psi}\psi\rangle = -\frac{D_\sigma(0) \Delta}{2g_s} . \quad (2.22)$$

For the mesonic polarization diagrams we get:

$$\begin{aligned} \delta\Pi_M^{(a)}(q) &= \frac{i}{2} \int \frac{d^4p}{(2\pi)^4} \sum_{M_1 M_2} \Gamma_{M, M_1, M_2}(q, p) D_{M_1}(p) \Gamma_{M, M_1, M_2}(-q, -p) D_{M_2}(-p - q) , \\ \delta\Pi_M^{(b)}(q) &= -i \int \frac{d^4p}{(2\pi)^4} \sum_{M_1} \Gamma_{M, M_1, M_1, M}(q, p, -p) D_{M_1}(p) , \\ \delta\Pi_M^{(c)}(q) &= -\frac{i}{2} \int \frac{d^4p}{(2\pi)^4} \sum_{M_1} \Gamma_{M, M_1, M, M_1}(q, p, -q) D_{M_1}(p) , \\ \delta\Pi_M^{(d)}(q) &= \frac{i}{2} \Gamma_{M, M, \sigma}(q, -q) D_\sigma(0) \int \frac{d^4p}{(2\pi)^4} \sum_{M_1} \Gamma_{M_1, M_1, \sigma}(p, -p) D_{M_1}(p) , \\ &= -i \Gamma_{M, M, \sigma}(q, -q) D_\sigma(0) \Delta . \end{aligned} \quad (2.23)$$

The symmetry factor of  $1/2$  for  $\delta\Pi_M^{(c)}$  and  $\delta\Pi_M^{(d)}$  has the same origin as in Eq. (2.20). Similarly in  $\delta\Pi_M^{(a)}$  we had to correct for the fact that the exchange of  $M_1$  and  $M_2$  leads to identical diagrams.

For the further evaluation of Eqs. (2.20) to (2.23) we proceed in two steps. In the first step we calculate the intermediate RPA meson-propagators. Simultaneously we can calculate the quark triangles and box diagrams. One is then left with a meson loop which has to be evaluated in a second step.

The various sums in Eqs. (2.20) to (2.23) are, in principle, over all quantum numbers of the intermediate mesons. However, for most applications we expect that the most important contributions come from the pion, which is the lightest particle in the game. For instance, the change of the quark condensate at low temperatures should be dominated by thermally excited pions. Also, for a proper description of the  $\rho$ -meson width in vacuum we only need the two-pion intermediate state in diagram  $\delta\Pi_M^{(a)}$ . Other contributions to this diagram, i.e.  $\pi a_1$ ,  $\rho\sigma$ ,  $\rho\rho$  and  $a_1 a_1$  intermediate states, are much less important since the corresponding decay channels open far above the  $\rho$ -meson mass and - in the NJL model - also above the unphysical two-quark threshold. Hence, from a purely phenomenological point of view, it should be sufficient for many applications to restrict the sums in Eq. (2.23) to intermediate pions. However, in order to stay consistent with chiral symmetry, we have to include intermediate sigma mesons as well. On the other hand, vector- and axial-vector mesons can be neglected without violating chiral symmetry. Since this leads to an appreciable simplification of the numerics we have restricted the *intermediate* degrees

of freedom to scalar and pseudoscalar mesons in the present paper. Of course, in order to describe a  $\rho$ -meson, we have to take vector couplings at the external vertices of the diagrams shown in Fig. 4.

### 3 Non-perturbative symmetry conserving schemes

#### 3.1 Axial Ward identities

The disadvantage of the  $1/N_c$ -expansion scheme is that it is perturbative. Although we have constructed the  $1/N_c$  corrections to the Hartree quark self-energy (Fig. 3) we did not selfconsistently include such diagrams in the gap equation. Since the iteration would produce terms of arbitrary orders in  $1/N_c$ , one is not allowed to do so in a strict expansion scheme. Therefore, all correction diagrams we have discussed in the previous section consist of ‘‘Hartree’’ quark propagators. This perturbative treatment should work rather well as long as the  $1/N_c$  corrections to the quark self-energy are small compared with the leading order, i.e. the constituent quark mass. On the other hand it is clear that the scheme must fail to describe the chiral phase transition, e.g. at finite temperatures. Here a non-perturbative treatment is mandatory.

Therefore, in this section, we want to follow a different strategy, exploiting the fact that the Goldstone theorem is basically a consequence of Ward identities: Consider an external axial current  $j_{\mu 5}^a$  coupled to a quark. Then, in the chiral limit, the corresponding vertex function  $\Gamma_{\mu 5}^a$  is related to the quark propagator  $S(p)$  via the axial Ward-Takahashi identity

$$q^\mu \Gamma_{\mu 5}^a(p, q) = S^{-1}(p + q) \gamma_5 \tau^a + \gamma_5 \tau^a S^{-1}(p), \quad (3.1)$$

where  $p$  and  $p + q$  are the 4-momenta of the incoming and outgoing quark, respectively. Obviously, for a non-vanishing constituent quark mass, the r.h.s. of this equation remains finite even for  $q \rightarrow 0$ . Consequently  $\Gamma_{\mu 5}^a(p, q)$  must have a pole in this limit, which can be identified with the Goldstone boson. Moreover the explicit structure of the Goldstone boson can be constructed from the structure of the axial vertex function.

As a first example, let us start again from the Hartree gap equation (Eq. (2.2), Fig. 1) and construct the axial vertex function by coupling the propagator to an external axial current. This is illustrated in Fig. 6. In the upper line, the first term on the r.h.s. describes the coupling to the bare quark, corresponding to a bare vertex  $\gamma_\mu \gamma_5 \tau^a$ . In the second term, however, the current is coupled to a dressed quark, and therefore we have to use the same vertex function as on the l.h.s. of the equation:

$$\Gamma_{\mu 5}^a(p, q) = \gamma_\mu \gamma_5 \tau^a + \sum_M 2ig_M \Gamma_M \int \frac{d^4k}{(2\pi)^4} \text{Tr} [\Gamma_M S(k + q) \Gamma_{\mu 5}^a(k, q) S(k)]. \quad (3.2)$$

Here  $S(k)$  denotes the quark propagator in the Hartree approximation. As in Eq. (2.2) the sum runs over all interaction channels, but of course only the pseudoscalar and the axial vector contributions do not vanish. Contracting Eq. (3.2) with  $q_\mu$  one obtains a linear equation for  $q_\mu \Gamma_{\mu 5}^a$ . One can easily verify that in the chiral limit the solution of this equation is given by the axial Ward-Takahashi identity, Eq. (3.1). To this end we

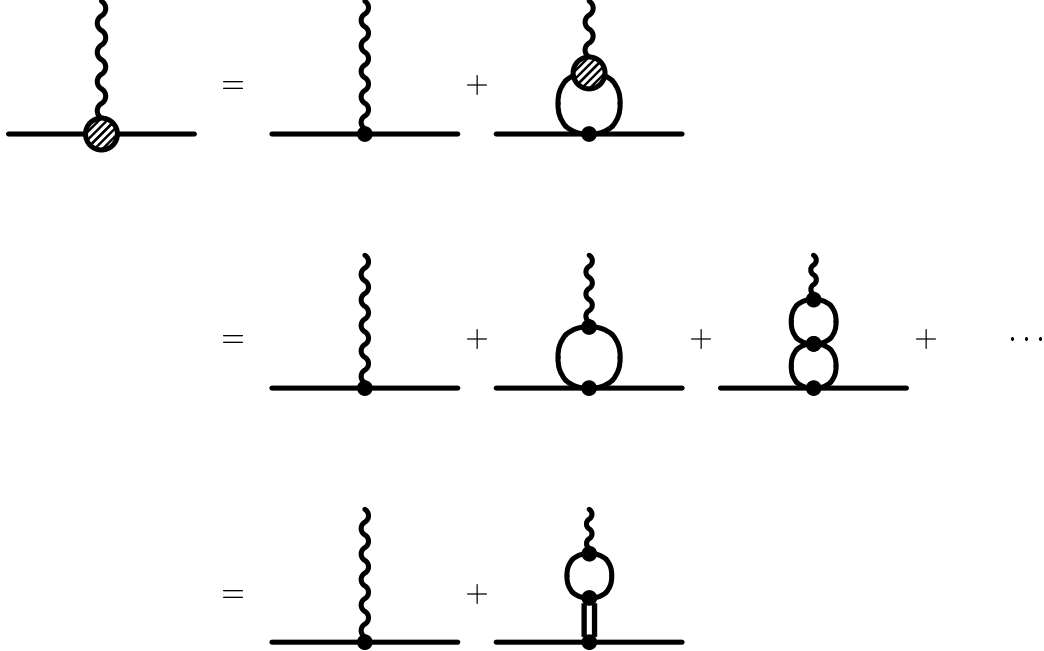


Figure 6: *Vertex function for an external axial current coupled to a “Hartree” quark.*

replace  $q_\mu \Gamma_{\mu 5}^a$  on both sides of the equation by the expressions given by Eq. (3.1) and check whether the results agree. On the r.h.s. the insertion of Eq. (3.1) basically amounts to removing one of the quark propagators from the loop. In this way the loop receives the structure of the quark self-energy and we can use the gap equation, Eq. (2.2) to simplify the expression. For  $m_0 = 0$  the result turns out to be equal to the l.h.s. of the equation, which proves the validity of the axial Ward-Takahashi in this scheme.

We have seen above, that this implies the existence of a massless Goldstone boson in the chiral limit. As illustrated in the second and third line of Fig. 6, the selfconsistent structure of Eq. (3.2) for the dressed vertex  $\Gamma_{\mu 5}^a$  leads to an iteration of the quark loop and an RPA pion emerges. Hence we can identify the Goldstone boson with an RPA pion.

Obviously the above procedure can be generalized to other cases: Starting from any given gap equation for the quark propagator we construct the vertex function to an external axial current by coupling the current in all possible ways to the r.h.s. of the equation. As long as the gap equation does not violate chiral symmetry this automatically guarantees the validity of the axial Ward-Takahashi identity and therefore the existence of a massless pion in the chiral limit. The structure of this pion can then be obtained from the structure of the vertex correction.

As an example we start from the extended gap equation depicted in the upper part of Fig. 7. There, in addition to the Hartree term, the quark is dressed by RPA mesons. These are defined in the same way as before (Fig. 2), but now selfconsistently using the quark propagator which results from the extended gap equation. Therefore the RPA pions are no longer massless in the chiral limit. However, following the strategy described above we can construct the consistent pion propagator. To that end we couple again an external axial current to both sides of the gap equation. The resulting equation for the vertex function is also shown in Fig. 7 (middle part). The additional term in the gap equation

leads to two new diagrams which were not present in Fig. 6: In the first the current couples to a quark-antiquark loop of the RPA meson while in the second it couples to the quark inside of the meson loop. Again, one can easily check that the vertex function and the quark propagator fulfill the axial Ward-Takahashi identity Eq. (3.1) in the chiral limit.

In principle one can construct the corresponding massless Goldstone boson from the quark-antiquark T-matrix given in the lower part of Fig. 7. In practice, however, this

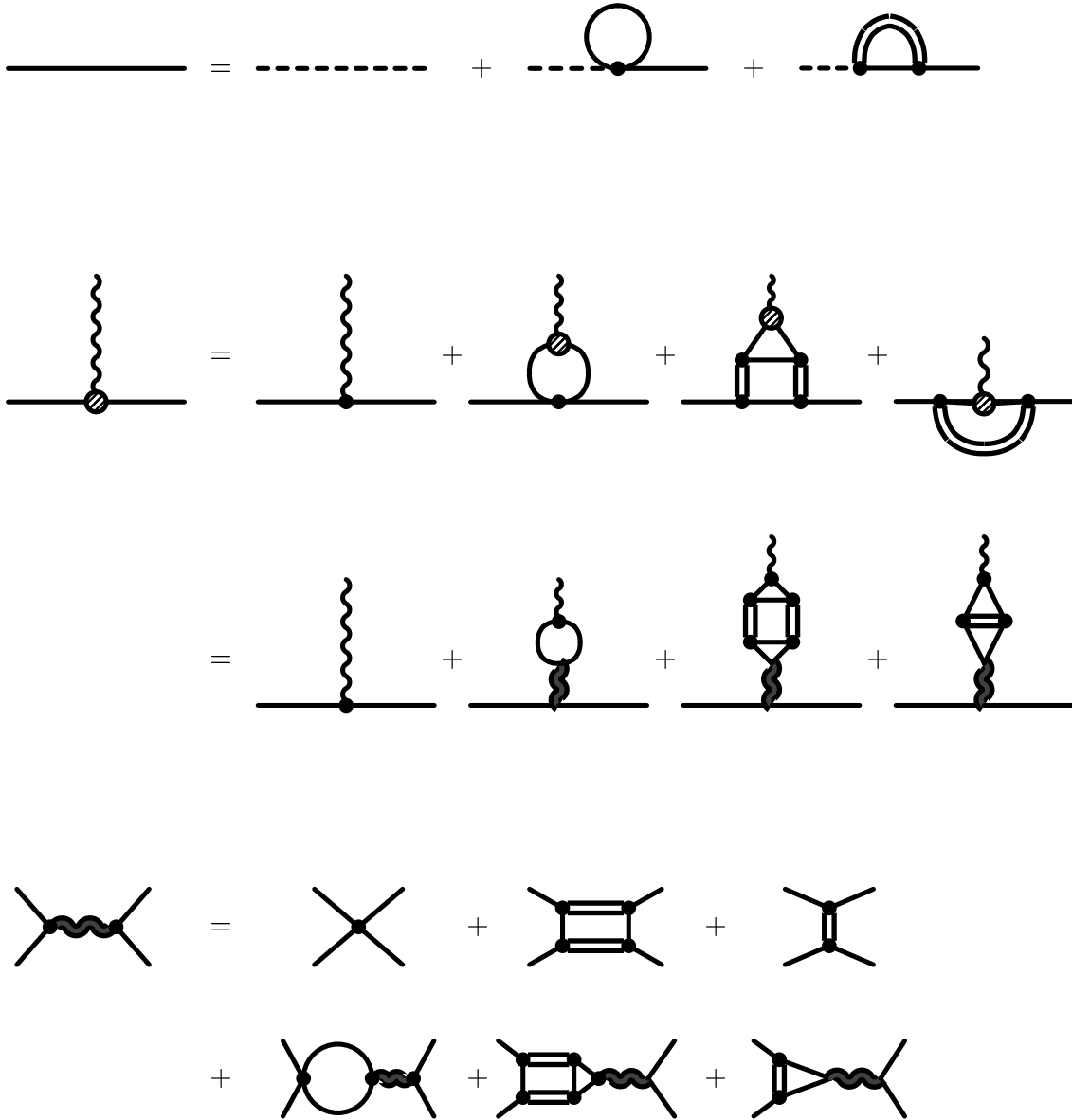


Figure 7: *Selfconsistent scheme with a non-local self-energy term: Gap equation (upper part), equation for the vertex function of an external current (middle) and the corresponding equation for the quark-antiquark T-Matrix (lower part). The double line denotes an RPA meson propagator (see Fig. 2), which is selfconsistently constructed from the dressed quark propagators of the present equation (solid line).*

is very difficult. In fact, already the solution of the extended gap equation is difficult, since the additional self-energy term is non-local, leading to a non-trivial 4-momentum dependence of the quark propagator. Note that this propagator has to be selfconsistently used for the calculation of the RPA-meson propagator. Therefore the authors of Ref. [14] suggested to drop the non-local terms, but to keep a particular class of local diagrams which arises from the combined iteration of the quark loop and the meson loop. This gap equation is shown in Fig. 8. Because of the restriction to local self-energy insertions, we will call this scheme the “local selfconsistent scheme” (LSS). It will be discussed in the next subsection.

### 3.2 The local selfconsistent scheme

The gap equation for the constituent quark mass in the local selfconsistent scheme (upper part of Fig. 8) reads

$$m = m_0 + \tilde{\Sigma}(m) = m_0 + \Sigma_H(m) + \delta\tilde{\Sigma}(m). \quad (3.3)$$

Here  $\Sigma_H$  is the Hartree contribution to the self-energy as defined in Eq. (2.2). The correction term  $\delta\tilde{\Sigma}$  corresponds to the third diagram on the r.h.s. of Fig. 8. We have explicitly indicated that the self-energy diagrams have to be evaluated selfconsistently at the quark mass  $m$ , which comes out of the equation. Because of the new diagram  $\delta\tilde{\Sigma}$ , this mass is in general different from the Hartree mass. However, since all diagrams in the LSS are constructed from the constituent quarks of Eq. (3.3), we prefer not to introduce a

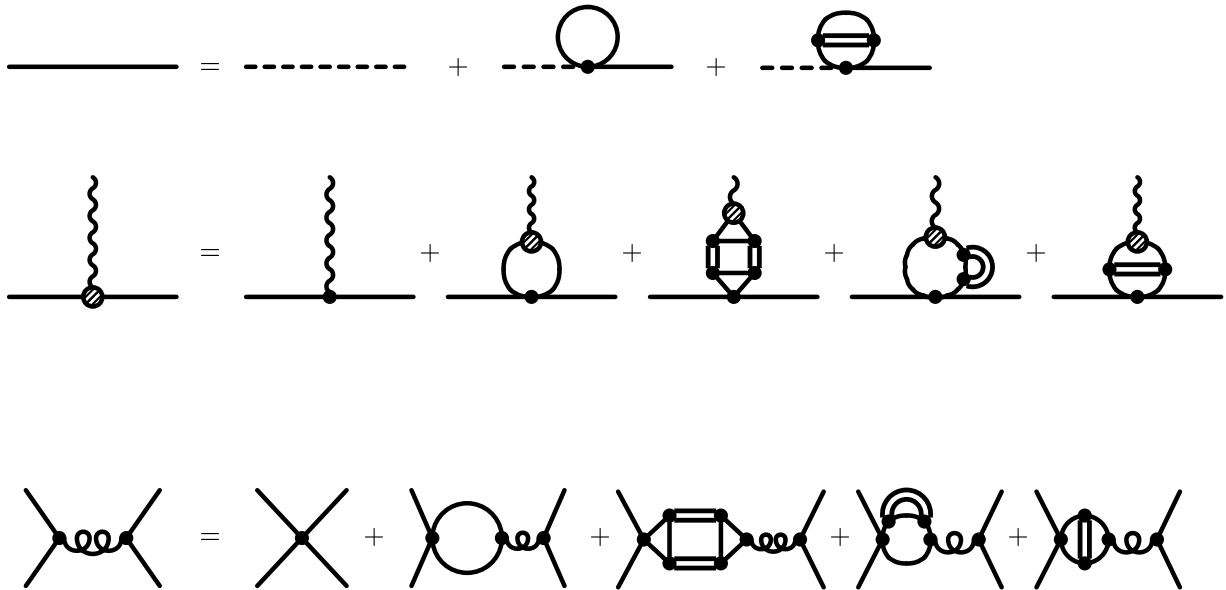


Figure 8: The “local selfconsistent scheme”: Gap equation (upper part), equation for the vertex function of an external current (middle) and the corresponding equation for the consistent meson propagator (lower part). The double line denotes an RPA meson propagator (see Fig. 2), which is selfconsistently constructed from the dressed quark propagators of the present equation (solid line).

new symbol for this mass. This has the advantage that we can also keep the notations for the quark propagator  $S(p) = (\not{p} - m)^{-1}$ , quark-antiquark loops, triangles etc. which we introduced earlier. The general structure of these diagrams is the same in all schemes we discuss in this article. Therefore we introduce the convention that in the  $1/N_c$ -expansion scheme  $m$  denotes the Hartree mass, while it denotes the solution of Eq. (3.3) in the LSS and all diagrams should be evaluated at that mass, unless stated otherwise.

The self-energy term  $\delta\tilde{\Sigma}$  consists of a quark loop dressed by an RPA-meson loop. The quark loop is coupled to the external quark propagators via the NJL point interaction. It can again be shown, that only the scalar interaction contributes. Hence  $\delta\tilde{\Sigma}$  is given by

$$\delta\tilde{\Sigma} = -2g_s \Delta, \quad (3.4)$$

where  $\Delta$  is the constant defined in Eq. (2.18).

Because of this additional self-energy diagram in the gap equation, the RPA is not the consistent scheme to describe mesons: In the chiral limit, RPA pions are no longer massless. Hence, in order to find the consistent meson propagators, we proceed in the way discussed in the previous subsection.

The equation for the axial vertex function is shown in the middle part of Fig. 8. Compared with the corresponding equation which follows from the Hartree approximation (Fig. 6) there are three extra terms. This leads to three additional polarization diagrams, which have to be iterated in the Bethe-Salpeter equation for the consistent meson propagator (lower part of Fig. 8).

Obviously these diagrams are identical to  $\delta\Pi_M^{(a)}$ ,  $\delta\Pi_M^{(b)}$  and  $\delta\Pi_M^{(c)}$ , which we defined in Sec. 2.2 (Fig. 4, Eq. (2.23)), i.e. the new meson propagators are given by

$$\tilde{D}_M(q) = \frac{-2g_M}{1 - 2g_M\tilde{\Pi}_M(q)}, \quad (3.5)$$

with

$$\tilde{\Pi}_M(q) = \Pi_M(q) + \sum_{k=a,b,c} \delta\Pi_M^{(k)}(q). \quad (3.6)$$

This structure agrees with the result of Ref. [14]. In that reference the scheme was motivated by a  $1/N_c$  expansion. However, one should stress again, that the selfconsistent solution of the gap equation mixes all orders in  $1/N_c$ . Moreover, the next-to-leading order self-energy correction term  $\delta\Sigma^{(b)}$  (cf. Fig. 3) is not contained in the gap equation of Fig. 8. Therefore the consistency of the scheme cannot be explained by  $1/N_c$ -arguments. In fact, our discussion shows that the structure of the consistent pion propagator can be derived from the gap equation without any reference to  $1/N_c$  counting.

On the other hand, if one performs a strict  $1/N_c$  expansion of the mesonic polarization diagrams up to next-to-leading order one exactly recovers the diagrams shown in Fig. 4 [14]. This is quite obvious for the diagrams  $\delta\Pi_M^{(a)}$  to  $\delta\Pi_M^{(c)}$ , which are explicitly contained in Eq. (3.6). Diagram  $\delta\Pi_M^{(d)}$ , which seems to be missing, is implicitly contained in the quark-antiquark loop via the next-to-leading order terms in the quark propagator, which arise from the extended gap equation.

In this sense, the LSS may be viewed as the simplest non-perturbative extension of the standard scheme which is consistent with the Goldstone theorem and which contains

all mesonic polarization diagrams up to next-to-leading order in  $1/N_c$ . However, since the diagram  $\delta\Sigma^{(b)}$  is not contained in the gap equation, this is not true for the quark condensate: If we evaluate Eq. (2.4) with the quark propagator of the present scheme, we obtain

$$\langle\bar{\psi}\psi\rangle = -\frac{\Sigma_H}{2g_s} = -\frac{m - m_0}{2g_s} - \Delta. \quad (3.7)$$

Performing a strict  $1/N_c$  expansion of this expression and only keeping the next-to-leading order term one does not recover Eq. (2.22) but only the contribution of  $\delta\Sigma^{(a)}$ . This might be the reason why the authors of Ref. [14] determine the quark condensate as

$$\langle\bar{\psi}\psi\rangle = -\frac{\tilde{\Sigma}}{2g_s} = -\frac{m - m_0}{2g_s}. \quad (3.8)$$

In contrast to Eq. (3.7) this expression reduces to the perturbative result in a strict  $1/N_c$  expansion. Moreover, as we will discuss in Sec. 4.2, it is consistent with the Gell-Mann–Oakes–Renner relation. On the other hand, Eq. (3.8) does obviously not follow from Eq. (2.4) with the quark propagator of the present scheme. A possible resolution to this problem was given in Ref. [15], where the LSS was derived using functional methods. The meson propagators obtained in that way are identical to Eqs. (3.5) and (3.6), while the quark condensate is given by Eq. (3.8). This will be briefly discussed in the following subsection.

Finally, we would like to comment on the name “local selfconsistent scheme”, which we have introduced in order to distinguish this scheme from the perturbative  $1/N_c$  expansion. We call this scheme “selfconsistent” because the quark propagator, which is determined by the gap equation is selfconsistently used in the loops and the RPA-meson propagator on the r.h.s. of that equation. However, as we have seen, the scheme is not selfconsistent with respect to the mesons: The improved meson propagators given by Eqs. (3.5) and (3.6) are different from the RPA mesons which are used in the gap equation and hence as intermediate states in the mesonic polarization functions  $\delta\Sigma^{(a)}$  to  $\delta\Sigma^{(c)}$ . On the other hand, if we had used the improved mesons already in the gap equation, our method of Sec. 3.1 would have led to further mesonic polarization diagrams in order to be consistent with chiral symmetry. Obviously, the construction of an expansion scheme, which is selfconsistent for quarks and mesons, is an extremely difficult task.

### 3.3 One-meson-loop order in the effective action formalism

Both, the non-local selfconsistent scheme, which we briefly discussed in Sec. 3.1 (Fig. 7), and the local selfconsistent scheme can be derived from functional methods: The non-local selfconsistent scheme can be obtained as a  $\Phi$ -derivable theory [25, 26] if one includes the “ring sum” in the generating functional. The present section is devoted to a brief discussion on how the local selfconsistent scheme can be derived from a one-meson-loop approximation to the effective action. The interested reader is referred to Refs. [15, 27]. Here we will basically follow Ref. [15].

In this section we drop the vector and axial vector interaction and start from a Lagrangian which contains only scalar and pseudoscalar interaction terms:

$$\mathcal{L} = \bar{\psi}(i\cancel{\partial} - m_0)\psi + g_s [(\bar{\psi}\psi)^2 + (\bar{\psi}i\gamma_5\vec{\tau}\psi)^2]. \quad (3.9)$$



The partition function of the system can be expressed in terms of the path integral

$$Z = e^{-W} = \int \mathcal{D}(\psi^\dagger) \mathcal{D}(\psi) e^{-I(\psi^\dagger, \psi)}, \quad (3.10)$$

with the Euclidean action

$$I(\psi^\dagger, \psi) = \int d^4x_E \left\{ \psi^\dagger \gamma_0 (\partial_\tau \gamma_0 - i\vec{\gamma} \cdot \vec{\nabla} + m_0) \psi - g_s ((\psi^\dagger \gamma_0 \psi)^2 + (\psi^\dagger \gamma_0 i\gamma_5 \vec{\tau} \psi)^2) \right\}. \quad (3.11)$$

The integration is here over a Euclidean space-time volume  $d^4x_E$ , where  $\partial_\tau$  corresponds to  $i\partial_t$ . The standard procedure is now to bosonize the action by introducing auxiliary fields  $\Phi'_a$ ,  $a = \{0, 1, 2, 3\}$

$$Z = \int \mathcal{D}(\psi^\dagger) \mathcal{D}(\psi) \mathcal{D}(\Phi'_a) \exp \left\{ -I(\psi^\dagger, \psi) - \frac{1}{4g_s} \int d^4x_E (\Phi'_a + 2g_s \psi^\dagger \gamma_0 \Gamma_a \psi)^2 \right\}, \quad (3.12)$$

with  $\Gamma_a = (1, i\gamma_5 \vec{\tau})$ . Then the action contains only bilinear terms in the quark fields, so that they can be integrated out. After performing a shift of the auxiliary fields,  $\Phi_a = \Phi'_a + (m_0, \vec{0})$ , one finally arrives at the bosonized action

$$I(\Phi) = -Tr \ln S^{-1} + \frac{1}{4g_s} \int d^4x_E (\Phi^2 - 2m_0 \Phi_0 + m_0^2), \quad (3.13)$$

where  $S^{-1}$  is the Dirac operator

$$S^{-1} = \gamma_0 \partial_\tau - i\vec{\gamma} \cdot \vec{\nabla} + \Gamma_a \Phi_a. \quad (3.14)$$

The symbol  $Tr$  in Eq. (3.13) is to be understood as a functional trace and a trace over internal degrees of freedom like flavor, color and spin.  $Tr \ln S^{-1}$  is the quark-loop contribution. The imaginary part of this term vanishes for the  $SU(2)$  case and we can rewrite the action as:

$$I(\Phi) = -\frac{1}{2} Tr \ln S^{-1\dagger} S^{-1} + \frac{1}{4g_s} \int d^4x_E (\Phi^2 - 2m_0 \Phi_0 + m_0^2). \quad (3.15)$$

The effective action  $\Gamma(\Phi)$  is defined as Legendre transform of the generating functional  $W(j)$ . Its stationary point  $\langle \Phi_a \rangle$ , i.e.

$$\left. \frac{\delta \Gamma(\Phi)}{\delta \Phi_a} \right|_{\Phi_a = \langle \Phi_a \rangle} = 0, \quad (3.16)$$

represents the vacuum expectation values of the fields.

The quark condensate can be expressed via the expectation value of  $\Phi_0$ . It is given as

$$\langle \bar{\psi} \psi \rangle = \frac{\partial W}{\partial m_0} = -\frac{1}{2g_s} (\langle \Phi_0 \rangle - m_0). \quad (3.17)$$

Another important feature of the effective action is that the inverse propagators of the fields (in our case the propagators for  $\pi$ - and  $\sigma$ -mesons) can be generated in a symmetry conserving way by second-order derivatives

$$D_{ab}^{-1} = \frac{\delta^2 \Gamma(\Phi)}{\delta \Phi_a \delta \Phi_b}. \quad (3.18)$$

To obtain an expression for the effective action the path integral is evaluated using the saddle point approximation. The lowest-order contribution to the effective action is

$$\Gamma^{(0)}(\Phi) = I(\Phi) . \quad (3.19)$$

This corresponds to the mean-field (Hartree) approximation [27]. The vacuum expectation values of the fields in mean-field approximation coincide with the stationary point of the action  $I(\Phi)$ . This is obvious if one combines Eq. (3.16) and Eq. (3.19). Including quadratic mesonic fluctuations leads to the following expression for the effective action [27]:

$$\Gamma(\Phi) = I(\Phi) + \frac{1}{2} Tr \ln \left( \frac{\delta^2 I(\Phi)}{\delta \Phi_a \delta \Phi_b} \right) . \quad (3.20)$$

The second term in the above expression contains the mesonic fluctuations. As discussed in Ref. [27] the method is only meaningful if the second-order functional derivative which enters into this term is positive definite. Otherwise severe problems arise due to an ill-defined logarithm, which would then be complex. We will come back to this point in Sec. 5.2.

Determining the stationary point of the effective action in Eq. (3.20) leads to the following ‘‘gap equation’’ [15]

$$\langle \Phi_0 \rangle - m_0 - \Sigma_H(\langle \Phi_0 \rangle) - \delta \tilde{\Sigma}(\langle \Phi_0 \rangle) = 0 . \quad (3.21)$$

Here  $\Sigma_H$  and  $\delta \tilde{\Sigma}$  are the same functions we already defined in Eqs. (2.2) and (3.4) in the context of the Hartree- and the LSS gap equation. In fact, Eq. (3.21) is identical to the LSS gap equation, Eq. (3.3), if we identify  $\langle \Phi_0 \rangle$  with the LSS-constituent quark mass  $m$ .

In the same way we exactly recover the meson structure of the LSS if we evaluate Eq. (3.18) at the stationary point. This means, the ‘‘local selfconsistent scheme’’ which was constructed from a somewhat arbitrary starting point in Sec. 3.2 can be derived in a systematic way in the effective action formalism. However, the interpretation is different: As emphasized in Ref. [15], the solution of the gap equation is only the expectation value of the  $\Phi_0$  field and does *not* correspond to the pole of the quark propagator. This becomes clear if we look at the quark condensate, which is given by Eq. (3.17). The r.h.s. of this equation is identical to Eq. (3.8) and therefore different from Eq. (3.7), which was derived by taking the trace over what we called the ‘‘quark propagator’’ in Sec. 3.2.

Hence, within the effective action formalism, Eq. (3.8) is the correct expression for the quark condensate (in that approximation scheme), whereas the gap equation should not be interpreted as an equation for the corresponding inverse quark propagator. In the following, we will adopt this point of view. For simplicity, however, we will still call  $m$  a ‘‘constituent quark mass’’ and  $(\not{p} - m)^{-1}$  a ‘‘quark propagator’’, although this is not entirely correct.

## 4 Consistency with chiral symmetry

By construction, the LSS is consistent with axial Ward-Takahashi identities and hence – as discussed in Sec. 3.1 – with the Goldstone theorem. Since the mesonic polarization functions of the LSS contain all diagrams up to next-to-leading order of the  $1/N_c$ -expansion

scheme and the various contributions to the pion mass have to cancel order by order in the chiral limit, this implies that the  $1/N_c$  scheme discussed in Sec. 2.2 is also consistent with the Goldstone theorem.

Nevertheless, for the numerical implementation it is instructive, to show the consistency of the different schemes with chiral symmetry on a less formal level. Since most of the integrals which have to be evaluated are divergent and must be regularized one has to ensure that the various symmetry relations are not destroyed by the regularization. To this end, it is important to know how these relations emerge in detail. This will also enable us to perform approximations without violating chiral symmetry. As we will see in Sec. 5.2, this is very important for practical calculations within the LSS, which cannot be applied as it stands.

For both, the  $1/N_c$ -expansion and the LSS, we begin our discussion with the explicit proof of the Goldstone theorem. This was given first by Dmitrašinović et al. [14]. After that we discuss the Gell-Mann–Oakes–Renner (GOR) relation. This is of particular interest in the context of the proper definition of the quark condensate in the LSS (cf. Eqs. (3.7) and (3.8)).

## 4.1 $1/N_c$ -expansion

We begin with the  $1/N_c$ -expansion scheme. For the Goldstone theorem one has to show that, in the chiral limit, the inverse pion propagator vanishes at zero momentum,

$$2g_s \tilde{\Pi}_\pi(0) = 1 \quad \text{for } m_0 = 0. \quad (4.1)$$

As before we use the notation  $\tilde{\Pi}_\pi^{ab} = \delta_{ab} \tilde{\Pi}_\pi$ . The function  $\tilde{\Pi}_\pi^{ab}$  has been defined in Eq. (2.14). It consists of the RPA polarization loop  $\Pi_\pi^{ab}$  and the four  $1/N_c$ -correction diagrams  $\delta\Pi_\pi^{(k)ab}$ ,  $k = a, b, c, d$ . Restricting the calculation to the chiral limit and to zero momentum simplifies the expressions considerably and Eq. (4.1) can be proven analytically.

For the RPA loop one obtains

$$2g_s \Pi_\pi(0) = \frac{\Sigma_H}{m}. \quad (4.2)$$

This is the relation which guarantees the consistency of the Hartree + RPA scheme: In Hartree approximation we have  $m = m_0 + \Sigma_H$  and hence Eq. (4.1), is fulfilled by Eq. (4.2). Since the gap equation is not changed in the perturbative  $1/N_c$  expansion, this remains true, if we include the next-to-leading order. Therefore we have to show that the contributions of the correction terms add up to zero:

$$\sum_{k=a,b,c,d} \delta\Pi_\pi^{(k)}(0) = 0 \quad \text{for } m_0 = 0. \quad (4.3)$$

The correction terms  $\delta\Pi_\pi^{(k)}$  are defined in Eq. (2.23). Let us begin with diagram  $\delta\Pi_\pi^{(a)}$ . As mentioned above, we neglect the  $\rho$  and  $a_1$  subspace for intermediate mesons. Then one can easily see that the external pion can only couple to a  $\pi\sigma$  intermediate state. Evaluating

the trace in Eq. (2.17) for zero external momentum one gets for the corresponding triangle diagram:

$$\Gamma_{\pi,\pi,\sigma}^{ab}(0, p) = -\delta_{ab} 4N_c N_f 2m I(p) , \quad (4.4)$$

with  $a$  and  $b$  being isospin indices and the elementary integral

$$I(p) = \int \frac{d^4k}{(2\pi)^4} \frac{1}{(k^2 - m^2 + i\varepsilon)((k+p)^2 - m^2 + i\varepsilon)} . \quad (4.5)$$

Inserting this into Eq. (2.23) we find

$$\delta\Pi_\pi^{(a)ab}(0) = i\delta_{ab} \int \frac{d^4p}{(2\pi)^4} (4N_c N_f I(p))^2 4m^2 D_\sigma(p) D_\pi(p) . \quad (4.6)$$

Now the essential step is to realize that the product of the RPA sigma- and pion propagators can be converted into a difference [14],

$$D_\sigma(p) D_\pi(p) = i \frac{D_\sigma(p) - D_\pi(p)}{4N_c N_f 2m^2 I(p)} , \quad (4.7)$$

to finally obtain

$$\delta\Pi_\pi^{(a)ab}(0) = -\delta_{ab} 4N_c N_f \int \frac{d^4p}{(2\pi)^4} 2I(p) \left\{ D_\sigma(p) - D_\pi(p) \right\} . \quad (4.8)$$

The next two diagrams can be evaluated straightforwardly. One finds:

$$\begin{aligned} \delta\Pi_\pi^{(b)ab}(0) &= -\delta_{ab} 4N_c N_f \int \frac{d^4p}{(2\pi)^4} \left\{ D_\sigma(p) (I(p) + I(0) - (p^2 - 4m^2) K(p)) \right. \\ &\quad \left. + D_\pi(p) (3I(p) + 3I(0) - 3p^2 K(p)) \right\} , \\ \delta\Pi_\pi^{(c)ab}(0) &= -\delta_{ab} 4N_c N_f \int \frac{d^4p}{(2\pi)^4} I(p) \left\{ -D_\sigma(p) - D_\pi(p) \right\} . \end{aligned} \quad (4.9)$$

The elementary integral  $K(p)$  is of the same type as the integral  $I(p)$  and is defined in App. A.

Finally we have to calculate  $\delta\Pi_\pi^{(d)}(0)$ . According to Eq. (2.23), it can be written in the form

$$\delta\Pi_\pi^{(d)ab}(0) = -i\Gamma_{\pi,\pi,\sigma}^{ab}(0, 0) D_\sigma(0) \Delta . \quad (4.10)$$

For the constant  $\Delta$ , defined in Eq. (2.18), one obtains

$$\begin{aligned} \Delta &= 4N_c N_f m \int \frac{d^4p}{(2\pi)^4} \left\{ D_\sigma(p) (2I(p) + I(0) - (p^2 - 4m^2) K(p)) \right. \\ &\quad \left. + D_\pi(p) (3I(0) - 3p^2 K(p)) \right\} . \end{aligned} \quad (4.11)$$

Evaluating  $D_\sigma(0)$  in the chiral limit and comparing the result with Eq. (4.4) one finds that the product of the first two factors in Eq. (4.10) is simply  $\delta_{ab}/m$ , i.e. one gets

$$\delta\Pi_\pi^{(d)ab}(0) = \delta_{ab} \frac{\Delta}{m} . \quad (4.12)$$

With these results it can be easily checked that Eq. (4.3) indeed holds in this scheme.

As already pointed out, most of the integrals we have to deal with are divergent and have to be regularized. Therefore one has to make sure that all steps which lead to Eq. (4.3) remain valid in the regularized model. One important observation is that the cancellations occur already on the level of the  $p$ -integrand, i.e. before performing the meson-loop integral. This means that there is no restriction on the regularization of this loop. We also do not need to perform the various quark loop integrals explicitly but we have to make use of several relations between them. For instance, in order to arrive at Eq. (4.12) we need the similar structure of the quark triangle  $\Gamma_{\pi,\pi,\sigma}(0,0)$  and the inverse RPA propagator  $D_\sigma(0)^{-1}$ . Therefore all quark loops, i.e. RPA polarizations, triangles and box diagrams should be consistently regularized within the same scheme, whereas the meson loops can be regularized independently.

Going away from the chiral limit the pion receives a finite mass. To lowest order in the current quark mass it is given by the Gell-Mann–Oakes–Renner (GOR) relation,

$$m_\pi^2 f_\pi^2 = -m_0 \langle \bar{\psi}\psi \rangle. \quad (4.13)$$

However, in the  $1/N_c$ -expansion scheme we cannot expect, that the GOR relation holds in this form. In Sec. 2 we have calculated the quark condensate in leading order and next-to-leading order in  $1/N_c$ . Hence, to be consistent, we should also expand the l.h.s. of the GOR relation up to next-to-leading order in  $1/N_c$ :

$$m_\pi^{2(0)} f_\pi^{2(0)} + m_\pi^{2(0)} \delta f_\pi^2 + \delta m_\pi^2 f_\pi^{2(0)} = -m_0 \left( \langle \bar{\psi}\psi \rangle^{(0)} + \delta \langle \bar{\psi}\psi \rangle \right). \quad (4.14)$$

Here, similar to the notations we already introduced for the quark condensate,  $m_\pi^{2(0)}$  and  $f_\pi^{2(0)}$  denote the leading order and  $\delta m_\pi^2$  and  $\delta f_\pi^2$  the next-to-leading order contributions to the squared pion mass and the squared pion decay constant, respectively. Since the GOR relation holds only in lowest order in  $m_0$ , Eq. (4.14) corresponds to a double expansion:  $m_\pi^2$  has to be calculated in linear order in  $m_0$ ,  $f_\pi^2$  and  $\langle \bar{\psi}\psi \rangle$  in the chiral limit.

The leading-order and next-to-leading-order expressions for the quark condensate are given in Eqs. (2.5) and (2.22). The pion decay constant  $f_\pi$  is calculated from the one-pion to vacuum axial vector matrix element. Basically this corresponds to evaluating the mesonic polarization diagrams, Fig. 3, coupled to an external axial current and to a pion. This leads to expressions similar to Eqs. (2.6) and (2.23), but with one external vertex equal to  $\gamma^\mu \gamma_5 \frac{\tau^a}{2}$ , corresponding to the axial current, and the second external vertex equal to  $g_{\pi qq} i \gamma_5 \tau^b$ , corresponding to the pion. Here the  $1/N_c$ -corrected pion-quark coupling constant is defined as

$$g_{\pi qq}^{-2} = g_{\pi qq}^{-2(0)} + \delta g_{\pi qq}^{-2} = \frac{d\tilde{\Pi}_\pi(q)}{dq^2} \Big|_{q^2=m_\pi^2}, \quad (4.15)$$

analogously to Eq. (2.10). Now we take the divergence of the axial current and then use the relation

$$\gamma_5 \not{p} = 2m\gamma_5 + \gamma_5 S^{-1}(k+p) + S^{-1}(k) \gamma_5 \quad (4.16)$$

to simplify the expressions [14]. One finds:

$$f_\pi = g_{\pi qq} \left( \frac{\tilde{\Pi}_\pi(q) - \tilde{\Pi}_\pi(0)}{q^2} m + \frac{\Pi_\pi(q) - \Pi_\pi(0)}{q^2} D_\sigma(0) \Delta \right) \Big|_{q^2=m_\pi^2}. \quad (4.17)$$

In the chiral limit,  $q^2 = m_\pi^2 \rightarrow 0$ , Eqs. (2.10) and (4.15) can be employed to replace the difference ratios on the r.h.s. by pion-quark coupling constants. When we square this result and only keep the leading order and the next-to-leading order in  $1/N_c$  we finally obtain:

$$f_\pi^{2(0)} + \delta f_\pi^2 = m^2 g_{\pi qq}^{-2(0)} + \left( m^2 \delta g_{\pi qq}^{-2} + 2m D_\sigma(0) \Delta g_{\pi qq}^{-2(0)} \right). \quad (4.18)$$

For the pion mass we start from Eqs. (2.15) and (2.16) and expand the inverse pion propagator around  $q^2 = 0$ :

$$1 - 2g_s \tilde{\Pi}_\pi(0) - 2g_s \left( \frac{d}{dq^2} \tilde{\Pi}_\pi(q) \right) \Big|_{q^2=0} m_\pi^2 + \mathcal{O}(m_\pi^4) = 0. \quad (4.19)$$

To find  $m_\pi^2$  in lowest non-vanishing order in  $m_0$  we have to expand  $1 - 2g_s \tilde{\Pi}_\pi(0)$  up to linear order in  $m_0$ , while the derivative has to be calculated in the chiral limit, where it can be identified with the inverse squared pion-quark coupling constant, Eq. (4.15). The result can be written in the form

$$m_\pi^2 = \frac{m_0}{m} \frac{g_{\pi qq}^2}{2g_s} \left( 1 - \frac{D_\sigma(0)\Delta}{m} \right) + \mathcal{O}(m_0^2). \quad (4.20)$$

Finally one has to expand this equation in powers of  $1/N_c$ . This amounts to expanding  $g_{\pi qq}^2$ , which is the only term in Eq. (4.20) which is not of a definite order in  $1/N_c$ . One gets:

$$m_\pi^{2(0)} + \delta m_\pi^2 = m_0 \frac{m}{2g_s} \frac{g_{\pi qq}^{2(0)}}{m^2} - m_0 \frac{m}{2g_s} \frac{g_{\pi qq}^{2(0)}}{m^2} \left( g_{\pi qq}^{2(0)} \delta g_{\pi qq}^{-2} + \frac{D_\sigma(0)\Delta}{m} \right). \quad (4.21)$$

It can be seen immediately that the leading-order term is exactly equal to  $-m_0 \langle \bar{\psi} \psi \rangle^{(0)} / f_\pi^{2(0)}$ , as required by the GOR relation. Moreover, combining Eqs. (2.22), (4.18) and (4.21) one finds that the GOR relation in next-to-leading order, Eq. (4.14), holds in this scheme.

However, one should emphasize that this result is obtained by a strict  $1/N_c$ -expansion of the various properties which enter into the GOR relation and of the GOR relation itself. If one takes  $f_\pi$  and  $m_\pi$  as they result from Eqs. (4.17) and (4.20) and inserts them into the l.h.s. of Eq. (4.13) one will in general find deviations from the r.h.s. which are due to higher-order terms in  $1/N_c$ . In this sense one can take the violation of the GOR relation as a measure for the importance of these higher-order terms [19].

## 4.2 Local selfconsistent scheme

The proof of the Goldstone theorem in the LSS is very similar to that in the  $1/N_c$ -expansion scheme. Therefore, we can be brief, concentrating on the steps which are different.

Again we have to show the validity of Eq. (4.1). In the LSS the function  $\tilde{\Pi}_\pi$  is given by Eq. (3.6), i.e. it differs from to the corresponding function in the  $1/N_c$ -expansion scheme (Eq. (2.14)) by the fact, that diagram  $\delta \Pi_\pi^{(d)}$  is (formally) missing. (As we already discussed it is implicitly contained in the RPA diagram.) The other diagrams have the

same structure as before and we can largely use the results of the previous subsection. However, we should keep in mind, that the constituent quark mass is now given by the extended gap equation, Eq. (3.3). Therefore, the r.h.s. of Eq. (4.2) is different from unity in the chiral limit and RPA pions are not massless. This has important consequences for the practical calculations within this scheme, which will be discussed in greater detail in section 5.2.

Using Eqs. (4.8), (4.9) and (4.11) as well as Eq. (3.4) we get for the correction terms to the pion polarization function

$$\sum_{k=a,b,c} \delta\Pi_{\pi}^{(k)}(0) = -\frac{\Delta}{m} = \frac{\delta\tilde{\Sigma}}{2g_s m}. \quad (4.22)$$

Hence, together with the modified gap equation (3.3) we find

$$2g_s \tilde{\Pi}_{\pi}(0) = 1 - \frac{m_0}{m} \quad (4.23)$$

in agreement with Eq. (4.1).

The discussion concerning the regularization procedure can be repeated here. The structure of the proof again leads to the conclusion that we have to regularize the quark loops in the same way, whereas we have the freedom to choose the regularization for the meson loops independently.

Another important observation is that we, in both schemes, do not need the explicit form of the RPA propagators.  $D_{\sigma}(p)$  and  $D_{\pi}(p)$  only need to fulfill Eq. (4.7). Thus, approximations to the RPA propagators can be made as long as Eq. (4.7) remains valid.

For a non-vanishing current quark mass the pion mass is given by the GOR relation (Eq. (4.13)). To linear order in  $m_0$  this relation holds exactly in the LSS, if we choose the appropriate definition of the quark condensate. This will be demonstrated in the following.

For the pion decay constant  $f_{\pi}$  we follow the same steps as in the  $1/N_c$ -expansion scheme to arrive at the following expression:

$$f_{\pi} = g_{\pi qq} m \frac{\tilde{\Pi}_{\pi}(q) - \tilde{\Pi}_{\pi}(0)}{q^2} \Big|_{q^2=m_{\pi}^2}. \quad (4.24)$$

Here the modified pion-quark coupling constant is defined as

$$g_{\pi qq}^{-2} = \frac{d\tilde{\Pi}_{\pi}(q)}{dq^2} \Big|_{q^2=m_{\pi}^2}. \quad (4.25)$$

In the chiral limit,  $m_{\pi}^2 \rightarrow 0$ , the difference ratio on the r.h.s. of Eq. (4.24) can be replaced by the pion-quark coupling constant (Eq. (4.25)). This leads to the Goldberger-Treiman relation

$$f_{\pi} g_{\pi qq} = m. \quad (4.26)$$

Following the analogous steps which led us to Eq. (4.20) we find for the pion mass

$$m_{\pi}^2 = \frac{m_0}{m} \frac{g_{\pi qq}^2}{2g_s} + \mathcal{O}(m_0^2). \quad (4.27)$$

Multiplying this with  $f_\pi^2$  as given by Eq. (4.26) we get to linear order in  $m_0$ :

$$m_\pi^2 f_\pi^2 = m_0 \frac{\tilde{\Sigma}}{2g_s}. \quad (4.28)$$

Obviously this is consistent with the GOR relation (Eq. (4.13)) if the quark condensate is given by Eq. (3.8), but not if it is given by Eq. (3.7). In Sec. 3.3 we have seen that within the effective action formalism the quark condensate is given by Eq. (3.8). Therefore at this point we clearly see that the interpretation of  $m$  as a constituent quark mass, which would mean that we have to calculate the quark condensate according to Eq. (3.7), leads to a contradiction with the GOR relation. Therefore, in the numerical part, we will calculate the quark condensate according to Eq. (3.8).

## 5 Numerical results at zero temperature

In this section we present our numerical results at zero temperature. We begin with a brief description of the regularization scheme and then discuss peculiarities related to the solution of the gap equation in the LSS. After that we study the influence of mesonic fluctuations on quantities in the pion sector, thereby focusing on possible instabilities. Finally we perform a refit of these quantities within the  $1/N_c$ -expansion scheme and the LSS and apply the model to observables in the  $\rho$ -meson sector.

### 5.1 Regularization

Before we begin with the explicit calculation we have to fix our regularization scheme. As discussed in Sec. 4, all quark loops, i.e. the RPA polarization diagrams, the quark triangles and the quark box diagrams must be regularized in the same way in order to preserve chiral symmetry. We use Pauli-Villars-regularization with two regulators, i.e. we replace

$$\int \frac{d^4k}{(2\pi)^4} f(k; m) \longrightarrow \int \frac{d^4k}{(2\pi)^4} \sum_{j=0}^2 c_j f(k; \mu_j), \quad (5.1)$$

with

$$\mu_j^2 = m^2 + j \Lambda_q^2; \quad c_0 = 1, \quad c_1 = -2, \quad c_2 = 1. \quad (5.2)$$

Here  $\Lambda_q$  is a cutoff parameter.

The regularization of the meson loop (integration over  $d^4p$  in Eq. (2.23)) is not constrained by chiral symmetry and independent from the quark loop regularization. For practical reasons we choose a three-dimensional cutoff  $\Lambda_M$  in momentum space. In order to obtain a well-defined result we work in the rest frame of the “improved” meson. The same regularization scheme was already used in Refs. [19, 20].

### 5.2 Solution of the gap equation in the LSS

In contrast to the  $1/N_c$ -expansion scheme, where all diagrams are constructed from “Hartree” quarks, the LSS is based on the extended gap equation, Eq. (3.3). In Sec. 3.2



this equation was the starting point to find a consistent set of diagrams for the description of mesons. In fact, in Sec. 4.2 we have shown, that various symmetry relations, namely the Goldstone theorem, the Goldberger Treiman relation and the GOR relation hold in this scheme. It is not surprising, that the structure of the extended gap equation was needed to prove these relations. So far, all this has been done on a rather formal level. This section is now devoted to the explicit solution of the modified gap equation in the LSS. We will see, that this cannot be done in a straightforward manner and we are forced to a slight modification of the scheme.

In addition to the Hartree term  $\Sigma_H$ , Eq. (3.3) contains the term  $\delta\tilde{\Sigma}$ , which is a quark loop, dressed by RPA mesons (see Fig. 8). As already pointed out, these RPA mesons consist of quarks with the selfconsistent mass  $m$ , which is in general different from the ‘‘Hartree’’ mass  $m_H$ . Hence, the masses of these mesons are also different from the meson masses in the Hartree + RPA scheme. On the l.h.s. of Fig. 9 we have plotted the squared masses  $m_M^{(0)2}$  of the RPA pion (solid) and the RPA  $\sigma$ -meson (dashed) as functions of a trial constituent quark mass  $m'$ . An important observation is that the pion becomes tachyonic, i.e.  $m_\pi^{(0)2}$  becomes negative, for quark masses smaller than the Hartree quark mass. Strictly speaking this is only the case in the chiral limit, whereas for nonvanishing current quark masses,  $m_\pi^{(0)2}$  becomes negative slightly below the Hartree quark mass. A similar observation can be made for  $m_\sigma^{(0)2}$ , but only for  $m'$  much smaller than the Hartree mass. This observation of tachyonic RPA mesons is related to the point discussed in Sec. 3.3, that the meson-loop term in the effective action (second term of Eq. (3.20)) is no longer positive definite.

Tachyonic RPA mesons lead to a complex correction to the quark self-energy. Therefore the solution of the extended gap equation can only be real if it is larger than the Hartree mass. Otherwise it must be complex. To investigate this point we plot the difference between the l.h.s. and the r.h.s. of Eq. (3.3) as a function of the (real) trial

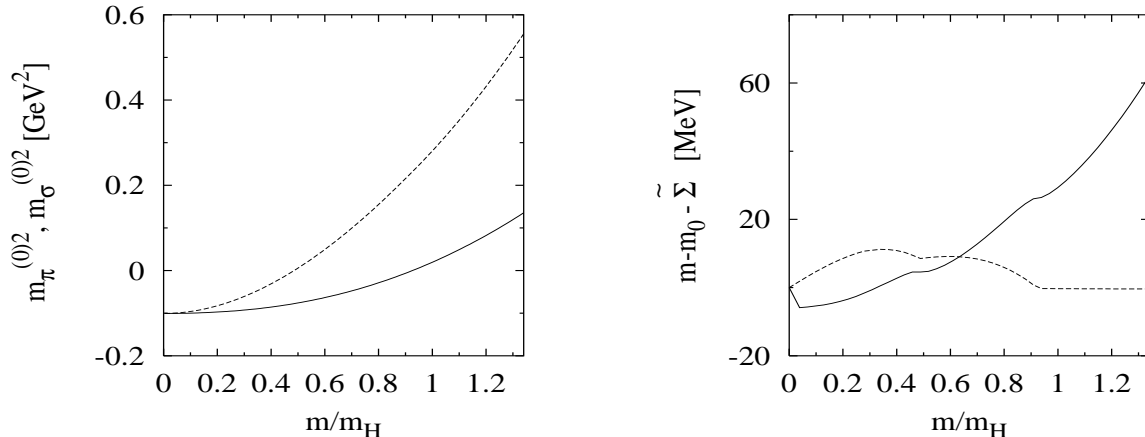


Figure 9: (Left) Squared pole masses of the pion (solid) and the  $\sigma$ -meson (dashed) in RPA as functions of a trial constituent quark mass  $m'$  in units of the Hartree quark mass. (Right) Difference  $m' - m_0 - \tilde{\Sigma}(m')$  between the l.h.s. and the r.h.s. of the LSS gap equation, Eq. (3.3), as a function of the trial constituent quark mass  $m'$ . The real part is denoted by the solid line, the imaginary part by the dashed line.

quark mass  $m'$ . This is shown in the right panel of Fig. 9. The solid line denotes the real part, the dashed line the imaginary part of  $m' - m_0 - \tilde{\Sigma}(m')$ . Obviously, below the Hartree quark mass, the self-energy indeed gets complex. Moreover, we see that there is no solution of the gap equation for real constituent quark masses. Hence, in principle, one should search for solutions of the gap equation in the complex plane. However, this would mean that the RPA mesons would also consist of quarks with complex masses. In this case, e.g. a reasonable description of the  $\rho$ -meson would be completely impossible, because its properties are mainly determined by intermediate pions.

Therefore, we prefer to perform an approximation, which was introduced in Ref. [15]. As discussed in Sec. 4.2 the symmetry properties of the LSS are not affected by approximations to the RPA meson propagators which preserve the validity of Eq. (4.7). The authors of Ref. [15] simply replace the RPA pion propagator in the extended gap equation

$$D_\pi(p) = -2g_s \left[ 1 - 2ig_s 4N_c N_f \int \frac{d^4k}{(2\pi)^4} \frac{1}{k^2 - m^2 + i\varepsilon} + 2ig_s(2N_c N_f) p^2 I(p) \right]^{-1} \quad (5.3)$$

by

$$D_\pi(p) = -2g_s \left[ \frac{m_0}{m} + 2ig_s 2N_c N_f p^2 I(p) \right]^{-1} \quad (5.4)$$

and analogously for the  $\sigma$ -propagator. The same replacements are performed for the RPA meson propagators in the correction terms  $\delta\Pi_M^{(k)}$  to the mesonic polarization diagrams. The RPA contribution  $\Pi_M$  itself, however, is not changed. In this way the solution of the gap equation and the masses of the intermediate mesons remain real. Moreover, in the chiral limit the intermediate pions are massless, as one can immediately see from Eq. (5.4).

The above replacements would be exact in the Hartree approximation (cf. Eq. (B.1)). The authors of Ref. [15] argue that the correction terms are suppressed because they are of higher orders of  $1/N_c$  (beyond next-to-leading order). In the LSS, this is a questionable argument because the selfconsistent solution of the gap equation mixes all orders of  $1/N_c$  anyway. Nevertheless this approximation preserves the validity of the various symmetry relations we have checked in Sec. 4.2.

In the following we will call this scheme, including the above replacements, the “local selfconsistent scheme” although it is strictly speaking only an approximation to the LSS as it was originally introduced in Sec. 3.2.

### 5.3 Meson-loop effects on quantities in the pion sector

In this subsection we want to study the influence of mesonic fluctuations on the quark condensate, the pion mass and the pion decay constant, both within the  $1/N_c$ -expansion scheme and within the LSS. Since the strength of the fluctuations is controlled by the meson cutoff  $\Lambda_M$ , we first keep all other parameters fixed and investigate how the above quantities change, when  $\Lambda_M$  is varied. For the  $1/N_c$ -expansion scheme this has been done in more detail in Ref. [19]. Later, in the next subsection, we will perform a refit of the parameters to reproduce the empirical values of  $\langle\bar{\psi}\psi\rangle$ ,  $m_\pi$  and  $f_\pi$ .

Our starting point is the Hartree + RPA scheme, which corresponds to  $\Lambda_M = 0$ . Here we obtain a reasonable fit ( $\langle\bar{\psi}\psi\rangle^{(0)} = -2 (241.1 \text{ MeV})^3$ ,  $m_\pi^{(0)} = 140.0 \text{ MeV}$  and

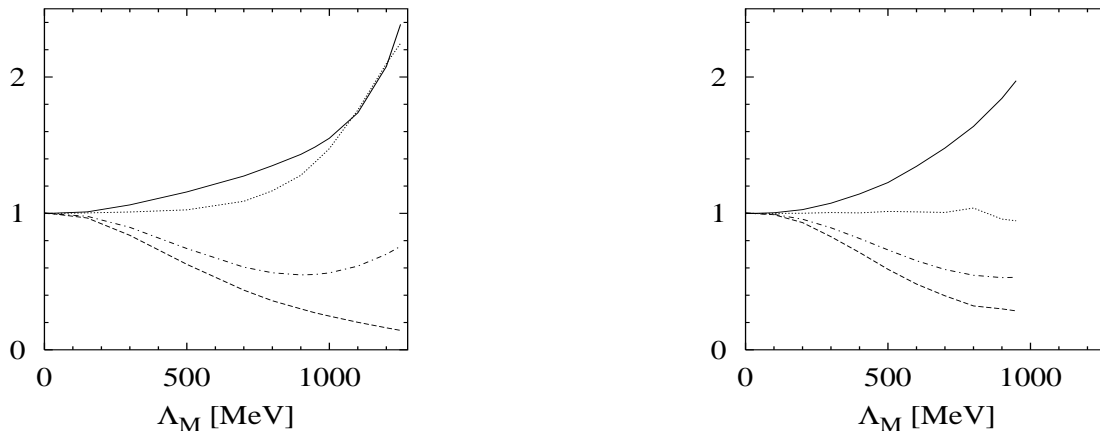


Figure 10: *The ratios  $m_\pi^2/m_\pi^{2(0)}$  (solid),  $f_\pi^2/f_\pi^{2(0)}$  (dashed),  $\langle\bar{\psi}\psi\rangle/\langle\bar{\psi}\psi\rangle^{(0)}$  (dashed-dotted) and the combination  $-m_0\langle\bar{\psi}\psi\rangle/m_\pi^2 f_\pi^2$  (dotted) as a function of the meson loop cutoff  $\Lambda_M$ . Left:  $1/N_c$ -expansion scheme, Right: LSS*

$f_\pi^{(0)} = 93.6$  MeV) with the parameters  $\Lambda_q = 800$  MeV,  $g_s\Lambda_q^2 = 2.90$  and  $m_0 = 6.13$  MeV. These parameters correspond to a relatively small “Hartree” constituent quark mass of 260 MeV.

Now we turn on the mesonic fluctuations by taking a non-zero meson cutoff  $\Lambda_M$ . All other parameters are kept constant at the values given above. The resulting behavior of  $m_\pi^2$ ,  $f_\pi^2$  and the quark condensate as a function of  $\Lambda_M$  is displayed in Fig. 10. The left panel corresponds to the  $1/N_c$ -expansion scheme, the right panel to the LSS. As one can see, in both schemes the mesonic fluctuations lead to a reduction of  $f_\pi$  (dashed lines) while  $m_\pi$  (solid) is increased. At smaller values of  $\Lambda_M$  the absolute value of the quark condensate decreases but goes up again for  $\Lambda_M \gtrsim 900$  MeV. This is also an effect which is found in both schemes.

In the Hartree + RPA scheme the quantities  $m_\pi^{2(0)}$ ,  $f_\pi^{2(0)}$  and  $\langle\bar{\psi}\psi\rangle^{(0)}$ , are in almost perfect agreement with the GOR relation, Eq. (4.13). As discussed in Sec. 4.1, the  $1/N_c$ -expansion scheme is consistent with the GOR relation up to next-to-leading order in  $1/N_c$ , but the relation is violated by higher-order terms. We therefore expect a less perfect agreement in this scheme, becoming worse with increasing values of  $\Lambda_M$ . In the LSS, on the other hand, the quantities should be in good agreement with the GOR (see Sec. 4.2).

These expectations are more or less confirmed by the results. In Fig. 10, the ratio of the r.h.s. and the l.h.s. of Eq. (4.13) is displayed by the dotted lines. In the  $1/N_c$ -expansion scheme (left panel) the relation holds within 30% for  $\Lambda_M \leq 900$  MeV. However, when the meson cutoff is further increased the deviation grows rapidly. This indicates that higher-order corrections in  $1/N_c$  become important in this regime and this perturbative scheme should no longer be trusted. In the LSS the agreement with the GOR is almost perfect.

In Fig. 10 the various curves are only shown up to  $\Lambda_M = 1250$  MeV for the  $1/N_c$ -expansion scheme and  $\Lambda_M = 950$  MeV for the LSS. For larger values of  $\Lambda_M$  a second, unphysical, pole with a residue of the “wrong” sign, emerges in the pion propagator.

This would correspond to an imaginary pion-quark coupling constant and hence an imaginary pion decay constant. Upon further increasing  $\Lambda_M$  the two poles merge and finally disappear from the positive real axis.

For the  $1/N_c$ -expansion scheme this has been discussed in more details in Ref. [19]. In that reference we suggested that the instabilities of the pion propagator might indicate an instability of the underlying ground state against mesonic fluctuations. In fact, it has been claimed by Kleinert and Van den Bossche [22] that there is no spontaneous chiral symmetry breaking in the NJL model as a consequence of strong mesonic fluctuations. Although this cannot be true in general if the strength of the mesonic fluctuations is controlled by an independent cutoff parameter  $\Lambda_M$  [19], this phenomenon might very well occur for large values of  $\Lambda_M$ . In other words: There could be some kind of “chiral symmetry restoration” at a certain value of the parameter  $\Lambda_M$ .

Clearly, this could not be studied within the  $1/N_c$ -expansion scheme where the mesonic fluctuations are built perturbatively on the Hartree ground state. In the LSS, however, where we encounter the same type of instabilities in the pion propagator, this question can be investigated more closely. To that end we consider the effective action Eq. (3.20), which describes the energy density of the system. It is explicitly given by

$$\begin{aligned} \Gamma(m') = & -4iN_cN_f \int \frac{d^4p}{(2\pi)^4} \ln\left(\frac{m'^2 - p^2}{m_0^2 - p^2}\right) + \frac{(m' - m_0)^2}{4g_s} \\ & - \frac{i}{2} \int \frac{d^4p}{(2\pi)^4} \{\ln(1 - 2g_s\Pi_\sigma(p)) + 3\ln(1 - 2g_s\Pi_\pi(p))\} + \text{const.} . \end{aligned} \quad (5.5)$$

The irrelevant constant can be chosen in such a way that  $\Gamma(0) = 0$ . The positions of the extrema of  $\Gamma(m')$  correspond to the solutions of the gap equation (3.3). In particular, the vacuum expectation value  $m$  is given by the value of  $m'$  at the absolute minimum of  $\Gamma$ . Note that, according to Eq. (3.8),  $m$  is proportional to the quark condensate, i.e. to the order parameter of chiral symmetry breaking. Hence, for a given value of  $\Lambda_M$ , chiral symmetry is spontaneously broken, if the absolute minimum of  $\Gamma$  is located at a non-zero value of  $m'$  and it is unbroken (“restored”) otherwise.

We perform the calculations in the chiral limit.<sup>†</sup> Our results for  $\Gamma(m')$  as a function of  $m'/m_H$  for different values of  $\Lambda_M$  are displayed in Fig. 11. For  $\Lambda_M = 0$  we find of course the minimum at  $m' = m_H = 260$  MeV, while there is a maximum at  $m' = 0$ . If there was indeed a “phase transition” due to mesonic fluctuations, this maximum should eventually convert to a minimum when  $\Lambda_M$  is increased. In fact, for  $\Lambda_M \lesssim 900$  MeV the results seem to point in this direction: In this regime the constituent quark mass  $m$  is reduced to about 30% of the Hartree mass. At the same time the “bag constant”  $B = \Gamma(0) - \Gamma(m)$  decreases from 48.7 MeV/fm<sup>3</sup> at  $\Lambda_M = 0$  to 0.8 MeV/fm<sup>3</sup> at  $\Lambda_M = 900$  MeV. However, upon further increasing  $\Lambda_M$ , both  $m$  and  $B$  go up again. In particular, the point  $\Gamma(0)$  always remains a local maximum: In the LSS we do not observe a “phase transition” due to strong mesonic fluctuations.

Here we should remark, that, according to the conjecture by Kleinert and Van den Bossche [22], the mesonic fluctuations do not restore the trivial vacuum in the NJL model,

---

<sup>†</sup>To be precise, we proceed as follows: Starting from the parameters given above, we keep the Hartree constituent quark mass,  $m_H = 260$  MeV, fixed, while  $m_0$  is reduced from 6.1 MeV to zero. Therefore the coupling constant is slightly enhanced from  $g_s\Lambda_q^2 = 2.90$  to  $g_s\Lambda_q^2 = 2.96$ .

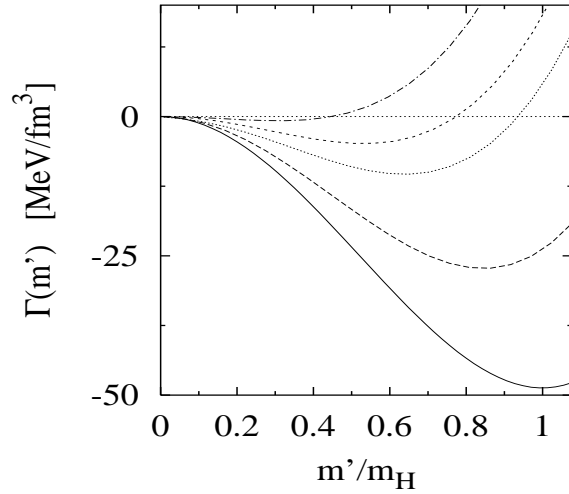


Figure 11: *Effective action  $\Gamma(m')$  as a function of  $m'/m_H$  in the LSS for different values of the meson cutoff  $\Lambda_M$ : 0 MeV (solid), 300 MeV (long-dashed), 500 MeV (dotted), 900 MeV (dashed-dotted) and 1200 MeV (short-dashed).*

but lead to a so-called pseudo-gap phase. (See also Ref. [28] for a critical discussion of this article.) In that phase the quarks still have a non-vanishing constituent mass, if the latter is identified with the vacuum expectation value of the *modulus* of the scalar field  $\Phi$  (cf. Sec. 3.3). Nevertheless chiral symmetry is not broken as the *phase* of the  $\Phi$  field is strongly fluctuating. An analogous phenomenon is well known from strong-coupling superconductors above  $T_c$  [29, 30], where Cooper pairs are formed, but do not condense. Obviously our above investigations, which focused on a the change of  $m$  assuming a uniform phase factor, cannot exclude a transition into a phase of this type. Here more refined investigations are needed to give a conclusive answer.

Another type of vacuum instability which is caused by unphysical poles of the RPA meson propagators has recently been discussed by Ripka [31]. Here “unphysical” means that these poles are located in regions of the complex plane, where they are forbidden by microcausality. Ripka stated, that they are induced by the regulator scheme, in his case a 4-momentum cutoff or a Gaussian form factor. In fact, the RPA meson propagators have this unphysical feature for most of the known regulator schemes, such as proper-time regularization, subtracted dispersion relations, dimensional regularization or, as mentioned above, a 4-momentum cutoff. A 3-momentum cutoff and Pauli-Villars-regularization in the form we use it (cf. appendix B) are exceptions. On the other hand, due to Pauli-Villars regulators, the imaginary part of the quark loops can have the wrong sign in some kinematical regions and we cannot rule out that the instabilities we find for the pion propagator are related to this. This supposition is corroborated by the fact that these instabilities could be traced back to the imaginary part of the diagram  $\delta\Pi^{(b)}$  (see Fig. 4) which has the “wrong” sign and which becomes large at large values of  $\Lambda_M$  [19]. Further investigations are needed, however, to clarify this point.

Recently a second (unphysical) pole in the pion propagator has also been found in

a non-local generalization of the NJL model [21]. The calculations indicate that these instabilities could probably be removed by including vector and axial vector intermediate states. This point is certainly worth a closer examination. In any case, at least in the  $1/N_c$ -expansion scheme we found [20] that with a reasonable fit of all parameters we are far away from the region where these instabilities occur. We will come back to this point in Sec. 5.5.

## 5.4 Parameter fit in the pion sector

In the previous subsection we did not change the parameters which were determined in the Hartree + RPA scheme by fitting  $f_\pi^{(0)}$ ,  $m_\pi^{(0)}$  and  $\langle\bar{\psi}\psi\rangle^{(0)}$ . Of course, if one wants to apply the model to describe physical processes a refit of these observables should be performed including the mesonic fluctuations. In Ref. [20] this was already done for the  $1/N_c$ -expansion scheme and we will now try to perform an analogous fit within the LSS. Of course, by fitting the above three observables, we cannot conclusively fix the five parameters of our model,  $g_s$ ,  $g_v$ ,  $\Lambda_q$ ,  $\Lambda_M$  and  $m_0$ . Therefore we try to proceed in a similar way as in Ref. [20]: For various values of  $\Lambda_M$  we fix the scalar coupling constant  $g_s$ , the current quark mass  $m_0$  and the quark-loop cutoff  $\Lambda_q$  to reproduce the empirical values of the pion mass,  $f_\pi$  and  $\langle\bar{\psi}\psi\rangle$ . Then, in the next subsection, we will try to fix the two remaining parameters, i.e. the vector coupling constant  $g_v$  and the meson cutoff  $\Lambda_M$ , by fitting the pion electromagnetic form factor in the time-like region, which is related, via vector meson dominance, to the  $\rho$ -meson propagator. Roughly speaking, this amounts to fitting the  $\rho$ -meson mass and its width. Since in our model the latter is due to intermediate RPA pions, we decided to fix the empirical value of  $m_\pi^{(0)}$ , not  $m_\pi$ , in order to get the correct threshold behavior. In Ref. [20] we found for the  $1/N_c$ -expansion scheme that the deviation is about 10%. As we will see below, in the LSS the difference is somewhat larger.

Of course, the  $\rho$ -meson can only be described reasonably if the unphysical  $q\bar{q}$ -threshold lies well above the peak in the  $\rho$ -meson spectral function. i.e. the constituent quark mass  $m$  should be larger than about 400 MeV. For that reason we try to increase the constituent quark mass as much as possible. Here we have some freedom as the empirical value of the quark condensate is not known very precisely. (Its absolute value is probably less than  $2(260 \text{ MeV})^3$ , which corresponds roughly to the upper limit extracted in Ref. [32] from sum rules at a renormalization scale of 1 GeV. Recent lattice results give  $\langle\bar{\psi}\psi\rangle = -2((231 \pm 4 \pm 8 \pm 6) \text{ MeV})^3$  [33].) On the other hand, since the correction term  $\delta\tilde{\Sigma}$  in the LSS gap equation, Eq. (3.3), contributes negatively to  $m$ , it is much more difficult in the LSS to obtain sufficiently large quark masses than in the  $1/N_c$ -expansion scheme.

Our results for the LSS are given in Table 2. For comparison we also summarize the results obtained in Ref. [20] within the  $1/N_c$ -expansion scheme (Table 1). In both tables we list five parameter sets (corresponding to five different meson cutoffs  $\Lambda_M$ ), together with the constituent quark mass  $m$ , the values of  $m_\pi$ ,  $f_\pi$  and  $\langle\bar{\psi}\psi\rangle$  and the corresponding RPA quantities. In the LSS the ‘‘RPA quantities’’ are calculated with the constituent quark mass  $m$  in order to represent the properties of the intermediate pion states. For completeness we also give the value of the Hartree mass  $m_H$  in Table 2 and the value of the quark condensate according to Eq. (3.7). We also show the ratio  $-m_0\langle\bar{\psi}\psi\rangle/m_\pi^2 f_\pi^2$ , which

$\Lambda_M / \text{MeV}$	0.	300.	500.	600.	700.
$\Lambda_q / \text{MeV}$	800.	800.	800.	820.	852.
$m_0 / \text{MeV}$	6.13	6.40	6.77	6.70	6.54
$g_s \Lambda_q^2$	2.90	3.07	3.49	3.70	4.16
$m / \text{MeV}$	260.	304.	396.	446.	550.
$m_\pi^{(0)} / \text{MeV}$	140.0	140.0	140.0	140.0	140.0
$m_\pi / \text{MeV}$	140.0	143.8	149.6	153.2	158.1
$f_\pi^{(0)} / \text{MeV}$	93.6	100.6	111.1	117.0	126.0
$f_\pi / \text{MeV}$	93.6	93.1	93.0	93.1	93.4
$\langle \bar{\psi}\psi \rangle^{(0)} / \text{MeV}^3$	$-2(241.1)^3$	$-2(249.3)^3$	$-2(261.2)^3$	$-2(271.3)^3$	$-2(287.2)^3$
$\langle \bar{\psi}\psi \rangle / \text{MeV}^3$	$-2(241.1)^3$	$-2(241.7)^3$	$-2(244.1)^3$	$-2(249.5)^3$	$-2(261.4)^3$
$-m_0 \langle \bar{\psi}\psi \rangle / m_\pi^2 f_\pi^2$	1.001	1.007	1.018	1.023	1.072

Table 1: The model parameters ( $\Lambda_M$ ,  $\Lambda_q$ ,  $m_0$  and  $g_s$ ) and the resulting values of  $m_\pi$ ,  $f_\pi$  and  $\langle \bar{\psi}\psi \rangle$  (together with the corresponding leading-order quantities), the constituent quark mass  $m$  in the  $1/N_c$ -expansion scheme. The ratio  $-m_0 \langle \bar{\psi}\psi \rangle / m_\pi^2 f_\pi^2$ , is also given.

$\Lambda_M / \text{MeV}$	0.	300.	500.	600.	700.
$\Lambda_q / \text{MeV}$	800.	800.	810.	820.	835.
$m_0 / \text{MeV}$	6.13	6.47	7.02	7.30	7.90
$g_s \Lambda_q^2$	2.90	3.08	3.44	3.71	4.52
$m_H / \text{MeV}$	260.	305.	390.	450.	600.
$m / \text{MeV}$	260.	278.2	320.0	355.7	468.4
$m_\pi^{(0)} / \text{MeV}$	140.0	139.9	140.0	139.7	140.0
$m_\pi / \text{MeV}$	140.0	145.1	156.3	164.5	182.7
$f_\pi^{(0)} / \text{MeV}$	93.6	96.7	103.6	108.4	120.0
$f_\pi / \text{MeV}$	93.6	93.2	92.9	92.9	92.8
$\langle \bar{\psi}\psi \rangle' / \text{MeV}^3$	$-2(241.1)^3$	$-2(244.7)^3$	$-2(254.3)^3$	$-2(261.9)^3$	$-2(277.3)^3$
$\langle \bar{\psi}\psi \rangle / \text{MeV}^3$	$-2(241.1)^3$	$-2(241.7)^3$	$-2(246.2)^3$	$-2(250.8)^3$	$-2(260.9)^3$
$-m_0 \langle \bar{\psi}\psi \rangle / m_\pi^2 f_\pi^2$	1.001	1.001	1.006	1.01	1.02

Table 2: The same as in Table 1 for the LSS. The quantity  $\langle \bar{\psi}\psi \rangle'$  denotes the quark condensate calculated according to Eq. (3.7).

would be equal to 1 if the GOR relation was exactly fulfilled. Note that the deviations in the  $1/N_c$ -expansion scheme are less than 10% (for  $\Lambda_M \leq 600$  MeV even less than 3%), indicating that higher-order corrections in  $1/N_c$  are small. In the LSS the deviations are considerably smaller, as already discussed in the previous subsection.

In both schemes we find that the constituent quark mass increases with an increasing meson cutoff  $\Lambda_M$ . In the  $1/N_c$ -expansion scheme for  $\Lambda_M \geq 500$  MeV the value of  $m$  is large enough to shift the  $q\bar{q}$ -threshold above the  $\rho$ -meson peak. Besides, it turns out that we can only stay below the limit of  $-2(260\text{MeV})^3$  for the quark condensate and simultaneously

reproduce the empirical value of  $f_\pi$  if the cutoff is not too large ( $\Lambda_M \lesssim 700$  MeV). In the LSS the region of values for  $\Lambda_M$  where on one hand the constituent quark mass is large enough and on the other hand the quark condensate stays below the limit is much more narrow. This can be seen from the values listed in Table 2. For a meson cutoff of  $\Lambda_M = 600$  MeV  $m$  is still too small and for  $\Lambda_M = 700$  MeV the quark condensate lies already slightly above the limit. The reason for this is obvious: In the LSS  $m$  and the quark condensate are directly related by Eq. (3.8) and therefore the mesonic fluctuations which lower the quark condensate also decrease the constituent quark mass. In the  $1/N_c$ -expansion scheme, on the contrary, the meson loop effects only contribute to the quark condensate and lower its value whereas  $m$  is kept fixed at its Hartree value.

## 5.5 Description of the $\rho$ -meson

As already pointed out, the parameter fit in the pion sector was not complete. It is clear, e.g., that the meson-loop cutoff  $\Lambda_M$  cannot be determined just by fitting the pion mass,  $f_\pi$  and  $\langle \bar{\psi}\psi \rangle$ , since these observables can already be reproduced in the Hartree + RPA scheme, i.e. without any meson-loop effects. We only found an upper limit of  $\Lambda_M \sim 700$  MeV in both schemes (see Tables 1 and 2). In Ref. [20] we therefore fixed the remaining parameters  $g_V$  and  $\Lambda_M$  for the  $1/N_c$ -expansion scheme in the  $\rho$ -meson sector. In this subsection we want to give a short summary of these results and then try to perform a similar fit for the LSS.

According to Eqs. (2.14) and (3.6), the polarization function of the  $\rho$ -meson reads:

$$\tilde{\Pi}_\rho^{\mu\nu,ab}(q) = \Pi_\rho^{\mu\nu,ab}(q) + \sum_k \delta\Pi_\rho^{(k)\mu\nu,ab}(q). \quad (5.6)$$

Here  $k$  runs over  $\{a, b, c, d\}$  in the  $1/N_c$ -expansion scheme and only over  $\{a, b, c\}$  in the LSS. Because of vector current conservation, the polarization function has to be transverse, i.e.

$$q_\mu \tilde{\Pi}_\rho^{\mu\nu,ab}(q) = q_\nu \tilde{\Pi}_\rho^{\mu\nu,ab}(q) = 0. \quad (5.7)$$

With the help of Ward identities it can be shown that these relations hold in both schemes, if we assume that the regularization preserves this property. This is the case for the Pauli-Villars regularization scheme, which was employed to regularize the RPA part  $\Pi_\rho$ . Together with Lorentz covariance this leads to Eq. (2.8) for the tensor structure of  $\Pi_\rho$ . On the other hand, since we use a three-dimensional sharp cutoff for the regularization of the meson loops, the correction terms  $\delta\Pi_\rho^{(k)\mu\nu,ab}$  are in general not transverse. However, as mentioned in Sec. 5.1, we work in the rest frame of the  $\rho$ -meson, i.e.  $\vec{q} = 0$ . In this particular case Eq. (5.7) is not affected by the cutoff and the entire function  $\tilde{\Pi}_\rho$  can be written in the form of Eq. (2.8):

$$\tilde{\Pi}_\rho^{\mu\nu,ab}(q) = \tilde{\Pi}_\rho(q) T^{\mu\nu} \delta_{ab} = \left( \Pi_\rho(q) + \sum_k \delta\Pi_\rho^{(k)}(q) \right) T^{\mu\nu} \delta_{ab}, \quad (5.8)$$

i.e. instead of evaluating all tensor components separately we only need to calculate the scalar functions  $\Pi_\rho = -1/3 g_{\mu\nu} \Pi_\rho^{\mu\nu}$  and  $\delta\Pi_\rho^{(k)} = -1/3 g_{\mu\nu} \delta\Pi_\rho^{(k)\mu\nu}$ .



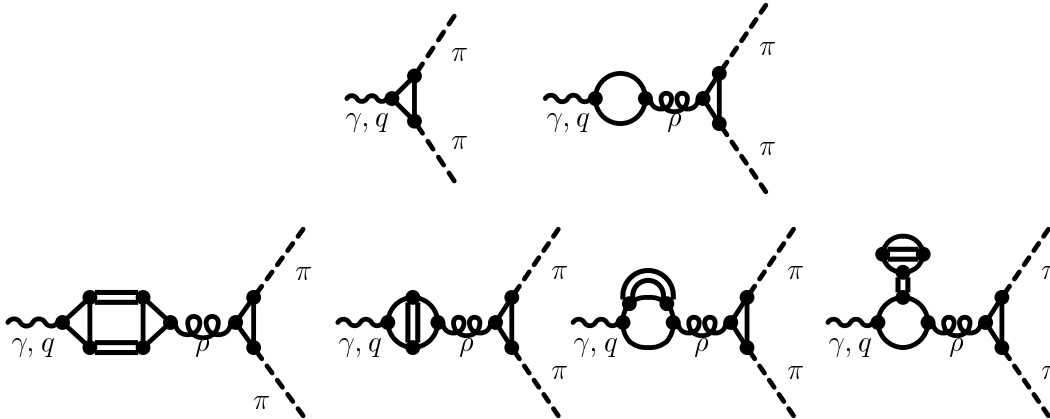


Figure 12: *Contributions to the pion electromagnetic form factor in the  $1/N_c$ -expansion scheme. The propagator denoted by the curly line corresponds to the  $1/N_c$ -corrected rho-meson, while the double lines indicate RPA pions and sigmas.*

A second consequence of vector current conservation is, that the polarization function should vanish for  $q^2 = 0$ . For the correction terms this is violated by the sharp cutoff. We cure this problem by performing a subtraction:

$$\sum_k \delta\Pi_\rho^{(k)}(q) \longrightarrow \sum_k \left( \delta\Pi_\rho^{(k)}(q) - \delta\Pi_\rho^{(k)}(0) \right). \quad (5.9)$$

Note, however, that already at the RPA level a subtraction is required, although the RPA part is regularized by Pauli-Villars. This is due to a rather general problem which is discussed in detail in App. B.

In Ref. [20] we have fixed  $g_v$  and  $\Lambda_M$  in the  $1/N_c$ -expansion scheme, by fitting the pion electromagnetic form factor,  $F_\pi(q)$ , in the time-like region, which is dominated by the  $\rho$ -meson. The diagrams we included in that calculations are shown in Fig. 12. The two diagrams in the upper part correspond to the standard NJL description of the form factor [34] if the full  $\rho$ -meson propagator (curly line) is replaced by the RPA one. Hence, the first improvement is the use of the  $1/N_c$ -corrected  $\rho$ -meson propagator in the  $1/N_c$ -expansion scheme. Since, in the standard scheme, the photon couples to the  $\rho$ -meson via a quark-antiquark polarization loop, in the  $1/N_c$ -expansion scheme we should also take into account the  $1/N_c$ -corrections to the polarization diagram for consistency. This leads to the diagrams in the lower part of Fig. 12. On the other hand the external pions are taken to be RPA pions (i.e. mass  $m_\pi^{(0)}$  and pion-quark-quark coupling constant  $g_{\pi qq}^{(0)}$ ). This is more consistent with the fact that the  $\rho$ -meson is also dressed by RPA pions and, as discussed above, we have fitted  $m_\pi^{(0)}$  to the experimental value.

The numerical results for  $|F_\pi|^2$  as a function of the center-of-mass energy squared are displayed in the left panel of Fig. 13, together with the experimental data [35]. The theoretical curve was calculated with a meson cutoff of  $\Lambda_M = 600$  MeV, a vector coupling constant  $g_v = 1.6g_s$  and the other parameters,  $\Lambda_q$ ,  $g_s$  and  $m_0$  as listed in Table 1. This roughly corresponds to a best fit to the data [20]. Since we assumed exact isospin symmetry we can, of course, not reproduce the detailed structure of the form factor around  $0.61$  GeV<sup>2</sup>, which is due to  $\rho$ - $\omega$ -mixing. The high-energy part above the peak is somewhat

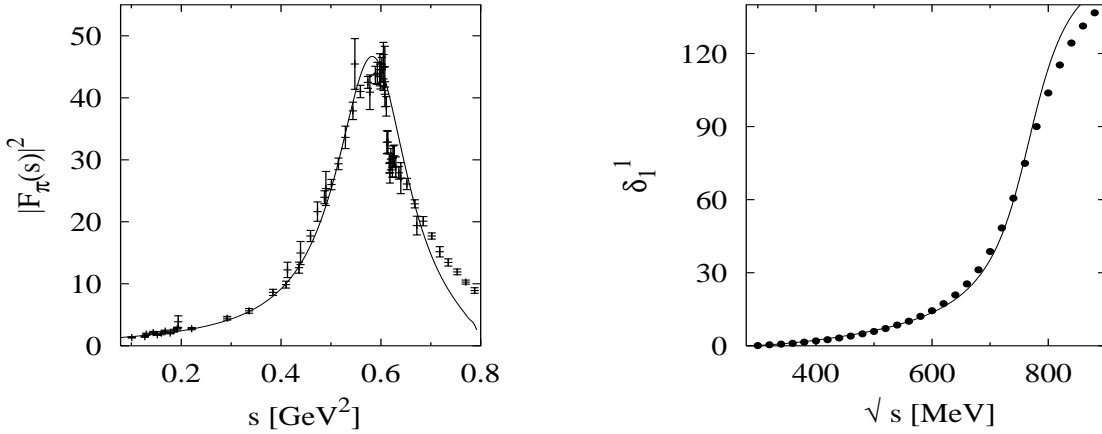


Figure 13: *The pion electromagnetic form factor (left panel) and the  $\pi\pi$ -phase shifts in the vector-isovector channel (right panel) for  $\Lambda_M = 600$  MeV and  $g_v = 1.6g_s$ . The other parameter values are taken from Table 1. The data points are taken from refs. [35] and [36], respectively.*

underestimated, mainly due to the sub-threshold attraction in the  $\rho$ -mesons channel below the  $q\bar{q}$ -threshold at  $s = 0.80$  GeV<sup>2</sup>. Probably the fit can be somewhat improved if we take a slightly larger meson cutoff, but we are not interested in fine-tuning here.

A closely related quantity is the charge radius of the pion, which is defined as

$$\langle r_\pi^2 \rangle = 6 \frac{dF_\pi}{dq^2} \Big|_{q^2=0}. \quad (5.10)$$

With the above parameter set we obtain a value of  $\langle r_\pi^2 \rangle^{1/2} = .61$  fm. It lies slightly below the experimental value,  $\langle r_\pi^2 \rangle^{1/2} = (0.663 \pm 0.006)$  fm [37].

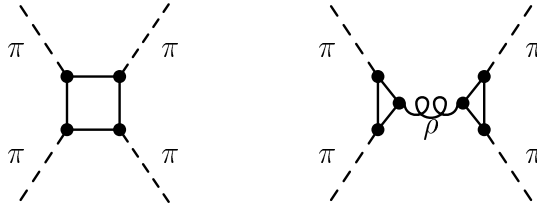


Figure 14: *Diagrams contributing to the  $\pi\pi$ -scattering amplitude: Quark box diagram (left) and  $s$ -channel  $\rho$ -meson exchange (right).*

One can also look at the  $\pi\pi$ -phase shifts in the vector-isovector channel. We include the diagrams shown in Fig. 14, i.e. the  $s$ -channel  $\rho$ -meson exchange and the direct  $\pi\pi$ -scattering via a quark box diagram. The latter has to be projected onto spin and isospin 1, which is a standard procedure. (For example, the analogous projection onto spin and isospin 0 can be found in Refs. [39, 40].) The result, together with the empirical data [36], is displayed in the right panel of Fig. 13. Since the main contribution comes from the  $s$ -channel  $\rho$ -meson exchange, it more or less confirms our findings for the form factor: below the  $\rho$ -meson peak a good fit of the data is obtained while, at higher energies, where  $q\bar{q}$ -threshold effects start to play a role, we slightly overestimate the data.

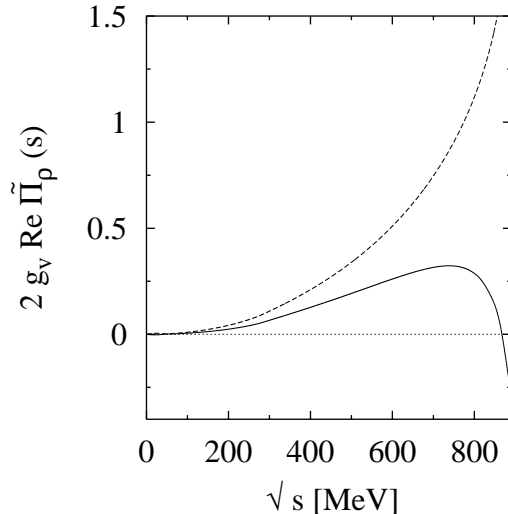


Figure 15: *Real part of the  $\rho$ -meson polarization function  $\tilde{\Pi}_\rho$  multiplied by  $2g_v = 17.6 \text{ GeV}^{-2}$  as a function of the energy  $\sqrt{s}$  in the rest frame of the meson. The dashed line corresponds to the  $1/N_c$ -expansion scheme with  $\Lambda_M = 600 \text{ MeV}$ , the solid line to the LSS with  $\Lambda_M = 700 \text{ MeV}$ . The other parameters are given in Table 1 and Table 2, respectively.*

Let us now turn to the LSS. As already discussed in the last paragraph of Sec. 5.4, there is not much room to vary the meson cutoff  $\Lambda_M$  in this scheme: On the one hand  $\Lambda_M$  is restricted to values  $\lesssim 700 \text{ MeV}$  by the fit to  $f_\pi$  and  $\langle \bar{\psi}\psi \rangle$  (see Table 2). On the other hand we only have a chance to get a realistic description of the  $\rho$ -meson if the constituent quark mass  $m$  is larger than at least  $400 \text{ MeV}$ . To achieve this, the meson cutoff cannot be much smaller than  $700 \text{ MeV}$ . This means,  $\Lambda_M$  is more or less fixed to this value and the only remaining parameter is the vector coupling constant  $g_v$ .

It turns out, however, that with  $\Lambda_M = 700 \text{ MeV}$  we run already into instabilities in the  $\rho$ -meson channel. These instabilities are of the same type as the instabilities in the pion channel, (see Sec. 5.3), but unfortunately emerge already at lower values of  $\Lambda_M$ . This can be seen in Fig. 15 where the real part of the of the  $\rho$ -meson polarization function  $\tilde{\Pi}_\rho$  multiplied by  $2g_v$  is plotted as a function of the energy  $\sqrt{s}$  in the rest frame of the meson. The LSS result corresponds to the solid line. For comparison we also show this function in the  $1/N_c$ -expansion scheme, using the ‘best-fit parameters’ given above (dashed curve).

According to Eqs. (2.15) and 3.5 the function  $2g_v \text{Re}\tilde{\Pi}_\rho$  has to become equal to 1 for  $\sqrt{s} \simeq m_\rho$ , crossing the line  $2g_v \text{Re}\tilde{\Pi}_\rho = 1$  from below. This is obviously the case in the  $1/N_c$ -expansion scheme. In this scheme,  $\text{Re}\tilde{\Pi}_\rho$  is a rising function and the above condition can be easily fulfilled with the appropriate choice of  $g_v$ . The situation is quite different in the LSS. Here  $\text{Re}\tilde{\Pi}_\rho$  has a maximum at  $\sqrt{s} \sim 740 \text{ MeV}$  and then steeply drops. Hence, if  $g_v$  is too small, the equation  $2g_v \text{Re}\tilde{\Pi}_\rho = 1$  has no solution at all (see Fig. 15). On the other hand, for large values of  $g_v$  we get a “physical” solution at lower energies and an “unphysical” solution at higher energies. It is clear that none of these two scenarios would lead to a realistic description of the  $\rho$ -meson.

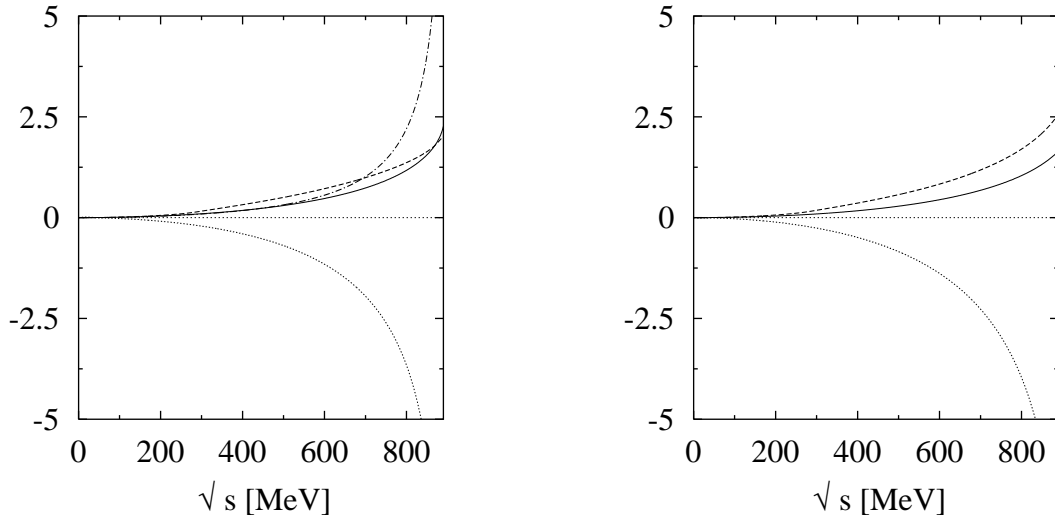


Figure 16: *RPA contribution  $2g_v\Pi_\rho$  (solid) and the various correction terms to  $2g_v\tilde{\Pi}_\rho$ :  $2g_v\delta\Pi_\rho^{(a)}$  (dashed),  $2g_v(\delta\Pi_\rho^{(b)} + \delta\Pi_\rho^{(c)})$  (dotted) and  $2g_v\delta\Pi_\rho^{(d)}$  (dashed-dotted). For all contributions we performed a subtraction, such that they vanish at  $\sqrt{s} = 0$ . The left panel corresponds to the  $1/N_c$ -expansion scheme, the right panel to the LSS. The model parameters are the same as in Fig. 15.*

One might wonder, why the results in the  $1/N_c$ -expansion scheme and in the LSS are so different. To answer this question we have separately plotted the various contributions to the polarization function in Fig. 16. The left panel corresponds to the results in the  $1/N_c$ -expansion scheme, the right panel to the LSS. One immediately sees that the unphysical behavior in the LSS is due to the sum of the diagrams  $\delta\Pi_\rho^{(b)}$  and  $\delta\Pi_\rho^{(c)}$  (dotted), which is the only negative contribution. In the  $1/N_c$ -expansion scheme these diagrams behave very similar. However, in this scheme their contribution is almost cancelled by the contribution of diagram  $\delta\Pi_\rho^{(d)}$ , which is not present in the LSS.

We should note that diagram  $\delta\Pi_\rho^{(a)}$ , which describes the two-meson intermediate state is well-behaved in both schemes. On the other hand the momentum dependence of all other diagrams is a pure quark effect, which could be related to the imaginary part of these diagrams above the (unphysical) two-quark threshold via dispersion relations. Hence, if we could manage to further push up the constituent quark mass, the momentum dependence of these contributions should become smaller and the instabilities should eventually vanish. Perhaps this is possible if further intermediate mesons, like  $\rho$  and  $a_1$  are included in the model.

## 6 Quark condensate at $T \neq 0$

It is expected, that at sufficiently large temperatures chiral symmetry, which is spontaneously broken in vacuum, gets restored. The quark condensate as an order parameter of chiral symmetry is well suited to study indications for (partial) chiral symmetry restoration. At low temperatures model independent results for the changes of the quark

condensate can be obtained from considering a gas of pions, which are the lightest particles and therefore the main degrees of freedom in this range. Approaching the phase transition we have to rely on model calculations or lattice data because we do not have any fundamental knowledge of the quark condensate at higher temperatures. Most of the results show a phase transition at a temperature of  $T_c \sim 150$  MeV.

Among others, the NJL model has been used to examine the behavior of the quark condensate as a function of temperature. Most of these investigations have been performed in the mean-field approximation [7, 8, 9, 10]. There one finds a second order phase transition with  $T_c \sim 150 - 200$  MeV. However one has to mention that these calculations suffer from the severe problem that the thermodynamics is generated exclusively by a gas of quarks. One consequence is that the low temperature behavior, which is driven mainly by pions, is completely missed. Although we cannot by-pass the fundamental problem of lack of confinement in the NJL model which in any case leads to the existence of a quark gas at non-zero temperature, we can hope to improve the situation at least at low temperatures via inclusion of mesonic degrees of freedom in a calculation beyond mean-field.

Therefore we begin with a closer look at the low-temperature behavior of the quark condensate at  $T \neq 0$ . After that we will discuss our numerical results within the  $1/N_c$ -expansion scheme and within the LSS.

## 6.1 Low-temperature behavior

In the chiral limit and at vanishing baryon density a strict low-temperature expansion in chiral perturbation theory leads to the following expression for the quark condensate [41]:

$$\langle \bar{\psi}\psi \rangle_T = \langle \bar{\psi}\psi \rangle \left( 1 - \frac{T^2}{8f_\pi^2} - \frac{T^4}{384f_\pi^4} + \dots \right). \quad (6.1)$$

Here  $\langle \bar{\psi}\psi \rangle$  denotes the quark condensate at zero temperature. The  $T^2$ -term represents the contributions from a pure pion gas, whereas the higher-order terms are due to interactions between the pions. It has been shown [41] that the  $T^2$ - and the  $T^4$ -term of this expansion are model independent results which follow from chiral symmetry alone. Thus in principle every chirally symmetric model, including the NJL model, should reproduce these terms. However, as  $f_\pi$  is of the order  $\sqrt{N_c}$ , we can see that they are of the order  $1/N_c$  and  $1/N_c^2$ , respectively. So a mean-field calculation, which corresponds to a restriction to leading in  $1/N_c$ , will not be able to reproduce these terms [23]. Indeed, NJL model calculations in mean-field show a much more flat behavior at low temperatures [10, 27]:

$$\langle \bar{\psi}\psi \rangle_T^{(0)} = \langle \bar{\psi}\psi \rangle^{(0)} \left( 1 - \frac{(2mT)^{3/2}}{\pi^{3/2} \langle \bar{\psi}\psi \rangle^{(0)}} e^{-\frac{m}{T}} + \dots \right). \quad (6.2)$$

Extending the calculations to next-to-leading order in  $1/N_c$  will allow us to reproduce the  $T^2$ -term. This will be demonstrated in the following.

Our calculations at non-zero temperature are performed within imaginary time formalism. Basically this amounts to replacing the energy integration in the various  $n$ -point functions by a sum over Matsubara frequencies. The explicit expressions are listed in

App. D. As there exists a preferred frame of reference in the heat bath, all dynamical quantities depend separately on energy and three-momentum. Hence in the following, a finite-temperature RPA propagator, for instance, will be denoted as  $D_M(\omega, \vec{p})$ . For scalar quantities, like masses or condensates at non-zero temperature we use a suffix  $T$  in order to distinguish them from the analogous quantities in vacuum (cf. Eqs. (6.1) and (6.2)).

In analogy to the vacuum expressions (Eqs. (2.5) and (2.22)) the quark condensate in next-to-leading order of the  $1/N_c$ -expansion scheme is given by

$$\langle \bar{\psi}\psi \rangle_T = \langle \bar{\psi}\psi \rangle_T^{(0)} + \delta \langle \bar{\psi}\psi \rangle_T = -\frac{m_T - m_0}{2g_s} - \frac{D_\sigma(0, 0)\Delta_T}{2g_s}. \quad (6.3)$$

As shown in Eq. (6.2), the leading-order term  $\langle \bar{\psi}\psi \rangle_T^{(0)}$  does not contribute to the change of the quark condensate to order  $T^2$ . Similarly, thermal effects in the  $\sigma$ -meson propagator can be neglected at low temperatures. Therefore we only need to consider the temperature dependence of  $\Delta_T$ . If standard techniques are used the sum over the Matsubara frequencies in Eq. (D.5) can be converted into a contour integral [42]:

$$\begin{aligned} \Delta_T = & 4iN_cN_f m_T \frac{1}{2\pi i} \int \frac{d^3p}{(2\pi)^3} \int_C \frac{dz}{e^{z/T} - 1} \left\{ D_\pi(z, \vec{p}) (3I(0, 0) - 3(z^2 - \vec{p}^2) K(z, \vec{p})) \right. \\ & \left. + D_\sigma(z, \vec{p}) (2I(z, \vec{p}) + I(0, 0) - (z^2 - \vec{p}^2 - 4m_T^2) K(z, \vec{p})) \right\}. \end{aligned} \quad (6.4)$$

At low temperatures, the main contribution to the temperature-dependent part of this integral comes from the lowest lying pion pole, as the other contributions are exponentially suppressed. In the chiral limit we can therefore approximate this part for low temperatures by

$$\Delta_T - \Delta = 4N_cN_f m \int \frac{d^3p}{(2\pi)^3} \frac{2}{e^{|\vec{p}|/T} - 1} \left\{ \frac{3}{2|\vec{p}|2N_cN_f} \right\}. \quad (6.5)$$

This integral can be evaluated analytically and we obtain:

$$\Delta_T - \Delta = m \frac{T^2}{2}. \quad (6.6)$$

The last step is to realize that in the chiral limit the vacuum  $\sigma$ -meson propagator can be expressed through the leading-order pion decay constant as

$$D_\sigma(0) = -\frac{1}{4f_\pi^2(0)} \quad (6.7)$$

(see Eqs. (B.4) and (B.9)). We finally obtain for the quark condensate in next-to-leading order at low temperatures:

$$\langle \bar{\psi}\psi \rangle_T = \langle \bar{\psi}\psi \rangle - \langle \bar{\psi}\psi \rangle^{(0)} \frac{T^2}{8f_\pi^2(0)} \quad (6.8)$$

Comparing this with the chiral perturbation theory result, Eq. (6.1), we see that we can in principle reproduce the  $T^2$ -term. Note, however, that the coefficient is given by the

quark condensate and the pion decay constant in leading order in  $1/N_c$ , according to a strict expansion of Eq. (6.1) up to next-to-leading order in  $1/N_c$ . The physical reason for this behavior is the fact that the  $1/N_c$  corrections to the quark condensate correspond to fluctuating RPA-mesons and hence the thermal corrections at low temperatures are due to thermally excited RPA pions in this model.

For the LSS, a similar result has been derived in Ref. [23]. In the chiral limit the authors find

$$\langle \bar{\psi}\psi \rangle_T = \langle \bar{\psi}\psi \rangle \left( 1 - \frac{T^2}{8f_\pi^{2(0)}} \right). \quad (6.9)$$

Here  $f_\pi^{2(0)}$  is understood as the RPA-pion decay constant, Eq. (B.9), but evaluated at the quark mass  $m$ , which follows from the LSS gap equation, Eq. (3.3). This corresponds to the fact that in the LSS the thermal corrections to the quark condensate at low temperatures are due to RPA pions which consist of LSS quarks.

## 6.2 Numerical results within the $1/N_c$ -expansion scheme

Our numerical results for the temperature behavior of the quark condensate within the  $1/N_c$ -expansion scheme are displayed in Fig. 17. The r.h.s. corresponds to a realistic parameter set with  $m_\pi^{(0)} = 140$  MeV (Table 1 with  $\Lambda_M = 600$  MeV), the l.h.s. to the chiral limit. The solid lines indicate the results obtained in next-to-leading order. For comparison we also show the leading order (dashed line) and the pure pion gas result (dotted).

We begin our discussion with the chiral limit. At low temperatures ( $T \lesssim 100$  MeV) our results show the behavior discussed in the previous subsection: The next-to-leading order result is in very good agreement with the pion gas result (Eq. 6.8), whereas the leading-order result remains almost constant. Therefore in this regime the extension of the NJL model to next-to-leading order in  $1/N_c$  leads to a considerable improvement. Since

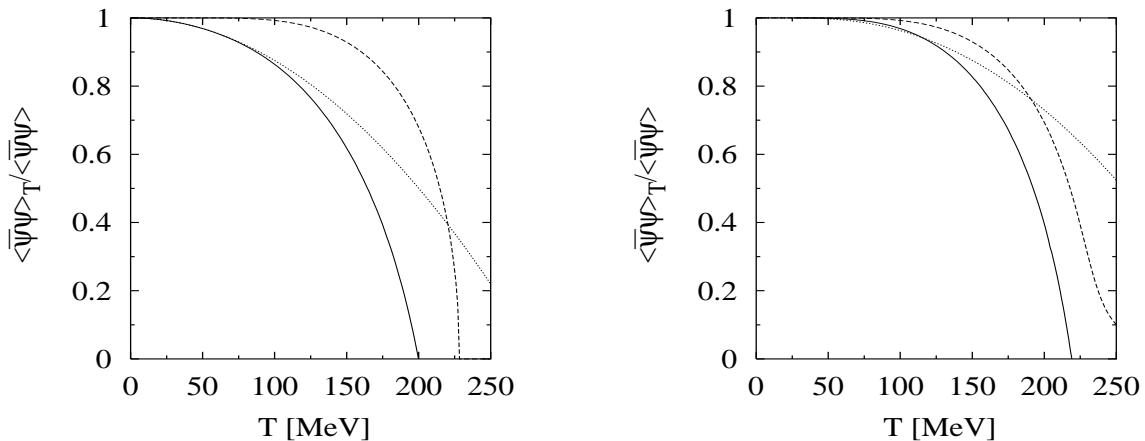


Figure 17: Quark condensate as a function of temperature, normalized to the vacuum value, in the chiral limit (left) and with  $m_\pi^{(0)} = 140$  MeV (right). Leading order in  $1/N_c$  (dashed line), next-to-leading order (solid line) and free pion gas (dotted line).

the unphysical quark degrees of freedom, which are in principle always present in the NJL model, are exponentially suppressed, the system is dominated by the (physical) pion degrees of freedom, which come about in next-to-leading order.

However, because of the much larger degeneracy factor (24 as compared to 3) we cannot avoid that effects due to thermally excited quarks become important at some temperature. In our present calculation this happens at about  $T \sim 100$  MeV. In a free gas approximation, this roughly corresponds to the temperature, at which the quark pressure becomes equal to the pion pressure.

At this point one might raise the question about the physical meaning of quark effects at these temperatures. In nature, quark degrees of freedom can only be excited above the deconfinement phase transition. In the NJL model there is no confinement and hence no deconfinement transition. However, lattice calculations [43] indicate that the deconfinement phase transition at finite temperature coincides with the chiral phase transition. One should therefore compare the temperature at which thermally excited quarks become important with the critical temperature for the chiral phase transition. From the above point of view, quark effects below the phase transition are either invisible or unphysical. On the other hand, at least close to the phase transition one might relax this strict position. In this regime one might think of a resonance gas with many degrees of freedom, which could be effectively described by a quark gas (“quark-hadron duality”).

Unfortunately, as already pointed out in Sec. 3, the perturbative treatment of the mesonic fluctuations does not allow for a description of the chiral phase transition. Although the quark condensate vanishes at  $T \sim 200$  MeV, this does not correspond to a true phase transition. (Note that the slope of the curve does not diverge at this point.) In any case, the applicability of the perturbative expansion scheme probably breaks down much earlier. Therefore we cannot give a definite answer to the question whether the thermally excited quarks become important near the phase transition or much below.

Our results with  $m_0 \neq 0$  are shown on the r.h.s. of Fig. 17. Since the RPA pions are now massive and therefore exponentially suppressed, the quark condensate as a function of  $T$  stays much more flat than in the chiral limit. Nevertheless, at low temperatures pions can still be most easily excited as they are the lightest particles. Therefore the next-to-leading order result (solid line) can be approximated quite well albeit not perfectly by the pure pion gas result (dotted) in this regime. The latter was calculated from the pressure  $p_\pi$  of a massive pion gas as

$$\langle \bar{\psi}\psi \rangle_T = \langle \bar{\psi}\psi \rangle + \langle \bar{\psi}\psi \rangle^{(0)} \frac{m_0}{f_\pi^{2(0)}} \frac{dp_\pi(T)}{dm_\pi^2(0)} \quad (6.10)$$

which can be easily derived with the help of the GOR relation.

Quark effects become important at almost the same temperature as in the chiral limit, at  $T \sim 100$  MeV.

### 6.3 Local selfconsistent scheme

Let us now compare the results of the previous subsection with the analogous calculations in the LSS. A study of the temperature dependence of the quark condensate within the LSS can also be found in Ref. [23]. Here we restrict ourselves to the chiral limit.



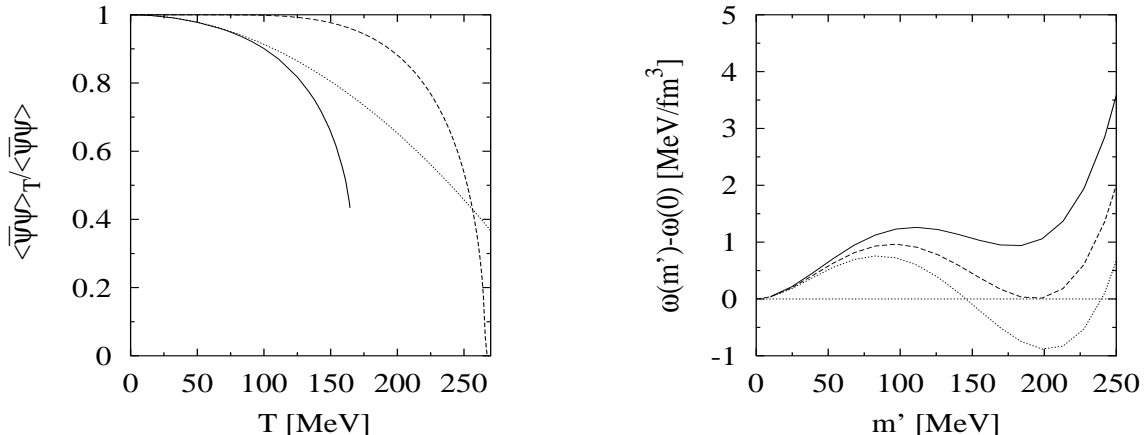


Figure 18: *Left: Quark condensate in the chiral limit as a function of temperature, normalized to the vacuum value, Hartree approximation (dashed), local selfconsistent scheme (solid) and free pion gas (dotted). Right: Thermodynamic potential per volume as a function of the constituent quark mass in the selfconsistent scheme with  $T = 163.9$  MeV (dotted),  $T = 164.5$  MeV (dashed) and  $165.3$  MeV (solid).*

Our results are shown on the l.h.s. of Fig. 18. The calculations have been performed using the parameters of Table 2 for  $\Lambda_M = 700$  MeV, but  $m_0 = 0$ . As discussed in Sec. 6.1, at low temperatures the model behaves again like a free pion gas (dotted line). Deviations from this behavior become visible at  $T \sim 100$  MeV which is quite similar to our observations in the  $1/N_c$ -expansion scheme.

In contrast to the  $1/N_c$ -expansion scheme, the treatment of the mesonic fluctuations in the LSS also allows an examination of the phase transition. With the present parameters it takes place at  $T_c = 164.5$  MeV which is considerably lower than in Hartree approximation, where we have  $T_c = 266.1$  MeV. Note, however, that about one third of this reduction can be attributed to the fact that the constituent quark mass  $m = 468.4$  MeV in the LSS is lower than the corresponding Hartree mass  $m_H = 600.0$  MeV. For  $m_H = 468$  MeV we would get a critical temperature of about 236 MeV in Hartree approximation. (It is also interesting to note, that the critical temperature in the LSS calculation almost coincides with the critical temperature  $T_c^{RPA} = 164.4$  MeV one obtains in Hartree approximation for the parameters fitted in the RPA, i.e.  $m = m_H = 260$  MeV.)

Whereas in Hartree approximation the phase transition is of second order, in the LSS the system undergoes a first-order phase transition, as already reported in Ref. [23]. This can be inferred from the thermodynamic potential  $\omega$ , which is displayed on the r.h.s. of Fig. 18 for different temperatures as a function of the constituent quark mass  $m'$ . At  $T = 164.5$  MeV one can clearly identify two degenerate minima at  $m' = 0$  and  $m' \neq 0$ , corresponding to a first-order phase transition at that temperature. One can ask whether this phenomenon depends on the strength of the mesonic fluctuations which can be controlled by the cutoff  $\Lambda_M$ . Varying this parameter we find that the discontinuity decreases with decreasing  $\Lambda_M$ , but even for very small values of the cutoff we encounter a first order phase transition.

Let us come back to the questions about the relevance of the unphysical quark degrees

of freedom. As already mentioned, deviations from the pure pion gas result become visible at  $T \sim 100$  MeV, which corresponds to about  $0.6T_c$ . At this temperature one would not expect quark effects to be present in nature. Furthermore, according to universality arguments, it is generally believed, that the finite-temperature chiral phase transition in QCD with two massless quarks is of second order [44]. This is based on the assumption that at  $T_c$  there are four massless bosonic degrees of freedom (three pions and one  $\sigma$ ) which determine the infrared behavior of the system. In this case QCD – but also the NJL model – should lie in the same universality class as the  $O(4)$ -model, which is known to have a second-order phase transition. Although some time ago it was claimed, that this argument might not hold if the boson fields are not elementary but composite [45], it is probably more likely that the first-order phase transition we observe is an artifact of the approximation scheme. In this context the application of renormalization group techniques to the NJL model would be extremely interesting.

## 7 Conclusions

We have investigated quark and meson properties within the Nambu–Jona-Lasinio model, including meson-loop corrections. These have been generated in two different ways. The first method is a systematic expansion of the self-energies in powers of  $1/N_c$  up to next-to-leading order [14, 19, 20]. In the second scheme, a local correction term to the standard Hartree self-energy is self-consistently included in the gap equation [14]. We therefore call it the “local selfconsistent scheme” (LSS). This scheme can also be derived as the one-meson-loop approximation to the effective action [15]. Both schemes, the  $1/N_c$ -expansion scheme and the LSS, are consistent with chiral symmetry, leading to massless pions in the chiral limit. For non-vanishing current quark masses the pion mass is consistent with the Gell-Mann–Oakes–Renner relation in the LSS. This is also true in the  $1/N_c$ -expansion scheme if one carefully expands both sides of the relation up to next-to-leading order in  $1/N_c$ .

The relative importance of the mesonic fluctuations is controlled by a parameter  $\Lambda_M$ , which cuts off the three-momenta of the meson loops. In both schemes we encounter instabilities in the pion propagator if the meson effects become too strong. In order to find out whether these instabilities are related to an unstable ground state [19, 22], leading to a “chiral restoration phase transition” at some critical value of  $\Lambda_M$ , we calculated the effective action of the LSS for increasing values of  $\Lambda_M$ . (Note, that such investigations are not possible within the  $1/N_c$ -expansion scheme, where mesonic fluctuations are included only perturbatively.) It turned out, that up to a certain value of  $\Lambda_M$  the system indeed seems to move towards a “phase transition”. However, when  $\Lambda_M$  is further increased the non-trivial ground state becomes again more stable and no phase transition takes place.

Of course, at the end, the value of  $\Lambda_M$ , together with the other parameters, has to be determined by fitting physical observables. The  $\rho$ -meson and related quantities are very well suited for this purpose, since the meson loops are absolutely crucial in order to include the dominant  $\rho \rightarrow \pi\pi$ -decay channel, while the Hartree+RPA approximation contains only unphysical  $q\bar{q}$ -decay channels. Here another problem, which constraints the possible choice of parameter values, becomes obvious: A priori it is not clear to what

extent these unphysical decay modes, which are an unavoidable consequence of the missing confinement mechanism in the NJL model, are still present in the region of the  $\rho$ -meson peak.

For the  $1/N_c$ -expansion scheme, the parameters have already been fixed in Ref. [20]. We obtained a reasonable fit of  $f_\pi$ ,  $\langle\bar{\psi}\psi\rangle$  and the pion electromagnetic form factor with a constituent quark mass of  $m = 446$  MeV. This means, the unphysical  $q\bar{q}$ -decay channel opens at 892 MeV, about 120 MeV above the maximum of the  $\rho$ -meson peak. Furthermore, the parameters of that fit are far away from the region, where the instabilities in the pion propagator emerge. In fact, we found only moderate changes in the pion and quark sector:  $f_\pi$  and  $\langle\bar{\psi}\psi\rangle$  are lowered by about 20% by the meson loop corrections, while the pion mass is increased by about 10%. This indicates that the  $1/N_c$  expansion converges rapidly and higher-order terms in the  $1/N_c$ -expansion are small.

Unfortunately we did not succeed to obtain a similar fit within the LSS. Since in this scheme the meson-loop effects lower the constituent quark mass as compared to the Hartree mass, it is much more difficult to evade the problem of unphysical  $q\bar{q}$ -decay channels in the vicinity of the  $\rho$ -meson peak. We found that a relatively large meson cutoff,  $\Lambda_M \sim 700$  MeV is needed in order to get the quark mass large enough and at the same time a fit for  $f_\pi$ . However, to our surprise for this cutoff the  $\rho$ -meson self-energy already suffers from stability problems, similar to those already discussed for the pion. As a result we are not able to get a reasonable description of the  $\rho$ -meson propagator and hence of the pion electromagnetic form factor within the LSS. It remains to be checked, whether these problems can be cured by taking into account additional intermediate states, like vector mesons and axial vector mesons or by different way of regularization.

In the last part of this article we have investigated the temperature dependence of the quark condensate. In both schemes the low-temperature behavior is consistent with lowest-order chiral perturbation theory, i.e. the temperature dependence arising from a free pion gas. This is a considerable improvement over the mean-field result, where the temperature dependence is entirely due to thermally excited quarks, i.e. unphysical degrees of freedom. At higher temperatures, however, thermal quark effects also become visible in the two extended schemes. We argued that this could be tolerable near the chiral phase boundary which is, according to lattice results, identical to the deconfinement phase boundary at non-zero temperatures.

Whereas the perturbative treatment of the mesonic fluctuations within the  $1/N_c$ -expansion scheme does not allow an examination of the chiral phase transition, this is possible in the LSS. For our model parameter set we found a critical temperature of 164.5 MeV. On the other hand, quark effects are visible already at a temperature of  $\sim 100$  MeV. Obviously this is still too early to be realistic. Maybe here the model can be improved by including additional intermediate meson states.

In agreement with Ref. [23] we found a first-order phase transition in that scheme. This contradicts the general belief that the non-zero temperature chiral phase transition in a model with two light flavors should be of second order and is probably an artifact of the approximation. Here further investigations, e.g. applying renormalization group techniques, would be very interesting.

## Acknowledgments

We are indebted to G.J. van Oldenborgh for his assistance in questions related to his program package FF (see <http://www.xs4all.nl/~gjvo/FF.html>), which was used in parts of our numerical calculations. We also thank G. Ripka, B.-J. Schaefer and M. Urban for illuminating discussions. This work was supported in part by the BMBF and NSF grant NSF-PHY98-00978.

## A Definition of elementary integrals

It is possible to reduce the expressions for the quark loops to some elementary integrals [46], see App. B and C. In this section we give the definitions of these integrals.

$$I_1 = \int \frac{d^4k}{(2\pi)^4} \frac{1}{k^2 - m^2 + i\varepsilon} , \quad (\text{A.1})$$

$$I(p) = \int \frac{d^4k}{(2\pi)^4} \frac{1}{(k^2 - m^2 + i\varepsilon)((k+p)^2 - m^2 + i\varepsilon)} , \quad (\text{A.2})$$

$$K(p) = \int \frac{d^4k}{(2\pi)^4} \frac{1}{(k^2 - m^2 + i\varepsilon)^2((k+p)^2 - m^2 + i\varepsilon)} , \quad (\text{A.3})$$

$$M(p_1, p_2) = \int \frac{d^4k}{(2\pi)^4} \frac{1}{(k^2 - m^2 + i\varepsilon)(k_1^2 - m^2 + i\varepsilon)(k_2^2 - m^2 + i\varepsilon)} , \quad (\text{A.4})$$

$$L(p_1, p_2, p_3) = \int \frac{d^4k}{(2\pi)^4} \frac{1}{(k^2 - m^2 + i\varepsilon)(k_1^2 - m^2 + i\varepsilon)(k_2^2 - m^2 + i\varepsilon)(k_3^2 - m^2 + i\varepsilon)} \quad (\text{A.5})$$

$$p_1^\mu M_1(p_1, p_2) + p_2^\mu M_1(p_2, p_1) = \int \frac{d^4k}{(2\pi)^4} \frac{k^\mu}{(k^2 - m^2 + i\varepsilon)(k_1^2 - m^2 + i\varepsilon)(k_2^2 - m^2 + i\varepsilon)} \quad (\text{A.6})$$

with  $k_i = k + p_i$ . The function  $M_1(p_1, p_2)$  can be expressed in terms of the other integrals:

$$M_1(p_1, p_2) = \frac{p_1 \cdot p_2 I(p_1) - p_2^2 I(p_2) + (p_2^2 - p_1 \cdot p_2) I(p_1 - p_2) + p_2^2 (p_1^2 - p_1 \cdot p_2) M(p_1, p_2)}{2((p_1 \cdot p_2)^2 - p_1^2 p_2^2)} , \quad (\text{A.7})$$

All integrals in Eqs. (A.1) to (A.6), are understood to be regularized. As described in Sec. 5.1 we use Pauli-Villars regularization with two regulators, i.e. we replace

$$\int \frac{d^4k}{(2\pi)^4} f(k; m) \longrightarrow \int \frac{d^4k}{(2\pi)^4} \sum_{j=0}^2 c_j f(k; \mu_j) , \quad (\text{A.8})$$

with

$$\mu_j^2 = m^2 + j \Lambda_q^2 ; \quad c_0 = 1, \quad c_1 = -2, \quad c_2 = 1 . \quad (\text{A.9})$$

One then gets the following relatively simple analytic expressions for the integrals  $I_1$ ,  $I(p)$  and  $K(p)$ :

$$I_1 = \frac{-i}{16\pi^2} \sum_j c_j \mu_j^2 \ln(\mu_j^2) \quad (\text{A.10})$$

$$I(p) = \frac{-i}{16\pi^2} \sum_j c_j \left( x_{j1} \ln(x_{j1}) + x_{j2} \ln(-x_{j2}) + x_{j1} \ln(-p^2 x_{j1}) + x_{j2} \ln(p^2 x_{j2}) \right) \quad (\text{A.11})$$

$$I(p=0) = \frac{-i}{16\pi^2} \sum_j c_j \ln(\mu_j^2) \quad (\text{A.12})$$

$$K(p) = \frac{-i}{16\pi^2} \sum_j c_j \frac{1}{2p^2(x_{j1} - x_{j2})} \left( -\ln(x_{j1}) - \ln(-x_{j1}) + \ln(x_{j2}) + \ln(-x_{j2}) \right) \quad (\text{A.13})$$

with

$$x_{j1,2} = \frac{1}{2} \pm \frac{1}{2} \sqrt{1 - \frac{4\mu_j^2}{p^2}}. \quad (\text{A.14})$$

An analytic expression for the three-point function (Eq. A.4) can be found in Refs. [47] and [48]. In certain kinematical regions the four-point function (eq. A.5) is also known analytically [47, 48].

## B RPA propagators

Using the definitions given in the previous section the gap equation (Eq. (2.2)) takes the form

$$m = m_0 + 2ig_s 4N_c N_f m I_1. \quad (\text{B.1})$$

Similarly one can evaluate the quark-antiquark polarization diagrams (Eq. (2.6)) and calculate the RPA meson propagators. The results for  $\sigma$ -meson and pion read:

$$D_\sigma(p) = \frac{-2g_s}{1 - 2ig_s 2N_c N_f (2I_1 - (p^2 - 4m^2) I(p))}, \quad (\text{B.2})$$

$$D_\pi(p) = \frac{-2g_s}{1 - 2ig_s 2N_c N_f (2I_1 - p^2 I(p))}. \quad (\text{B.3})$$

If we evaluate these propagators with the constituent quark mass in Hartree approximation we can simplify the above expressions with the help of the gap equation (Eq. B.1) to obtain:

$$D_\sigma(p) = \frac{-2g_s}{\frac{m_0}{m} + 2ig_s 2N_c N_f (p^2 - 4m^2) I(p)}, \quad (\text{B.4})$$

$$D_\pi(p) = \frac{-2g_s}{\frac{m_0}{m} + 2ig_s 2N_c N_f p^2 I(p)}. \quad (\text{B.5})$$

As discussed in Sec. 5.2, this form is also used for the internal meson propagators in the LSS.

A straight-forward evaluation of the vector and axial vector polarization diagrams gives

$$\Pi_\rho(p) = -i\frac{4}{3}N_c N_f (-2I_1 + (p^2 + 2m^2) I(p)), \quad (\text{B.6})$$

$$\Pi_{a_1}(p) = -i\frac{4}{3}N_c N_f (-2I_1 + (p^2 - 4m^2) I(p)). \quad (\text{B.7})$$

Because of vector current conservation  $\Pi_\rho$  should vanish for  $p^2 = 0$ . This is only true if

$$m^2 I(0) = I_1 , \quad (\text{B.8})$$

which is not the case if we regularize  $I(p)$  and  $I_1$  as described in App. A. This corresponds to the standard form of Pauli-Villars regularization in the NJL model [7]. Alternatively one could perform the replacement Eq. (5.1) for the entire polarization loop. In fact, this is more in the original sense of Pauli-Villars regularization [49]. Then the factor  $m^2$  in Eq. (B.6) should be replaced by a factor  $\mu_j^2$  inside the sum over regulators and one can easily show that Eq. (B.8) holds (see Eqs. (A.10) and (A.12)). However, this scheme would lead to even more severe problems: From the gap equation (Eq. B.1) we conclude that  $iI_1$  should be positive. On the other hand the pion decay constant in the chiral limit and in leading order in  $1/N_c$  is given by [7]

$$f_\pi^{2(0)} = -2iN_c N_f m^2 I(0) . \quad (\text{B.9})$$

which implies that  $im^2 I(0)$  should be negative. So irrespective of the regularization scheme Eq. (B.8) cannot be fulfilled if we want to get reasonable results for  $m$  and  $f_\pi^{(0)}$  at the same time. Therefore we choose the standard form of Pauli-Villars regularization in the NJL-model [7] and replace the term  $I_1$  in Eq. (B.6) by hand by  $m^2 I(0)$ . For consistency the  $a_1$  is treated in the analogous way. This leads to the following  $\rho$ - and  $a_1$ -meson propagator

$$D_\rho(p) = \frac{-2g_v}{1 + 2ig_v \frac{4}{3} N_c N_f (-2m^2 I(0) + (p^2 + 2m^2) I(p))} , \quad (\text{B.10})$$

$$D_{a_1}(p) = \frac{-2g_v}{1 + 2ig_v \frac{4}{3} N_c N_f (-2m^2 I(0) + (p^2 - 4m^2) I(p))} . \quad (\text{B.11})$$

## C Explicit expressions for the meson-meson vertices

In this section we list the explicit formulae for the meson-meson vertices. We restrict ourselves to those combinations which are needed for the calculations presented in this article.

We begin with the three-meson vertices  $\Gamma_{M_1, M_2, M_3}(q, p)$  (see Fig. 4):

$$\begin{aligned} -i\Gamma_{\sigma, \sigma, \sigma}(q, p) &= i2mN \left( I(p') + I(q) + I(p) + (4m^2 - \frac{1}{2}(p'^2 + p^2 + q^2))M(p, -q) \right) , \\ -i\Gamma_{\pi, \pi, \sigma}^{ab}(q, p) &= i2mN \delta_{ab} \left( I(p') + p \cdot q M(p, -q) \right) , \\ -i\Gamma_{\rho, \rho, \sigma}^{\mu\lambda, ab}(q, p) &= \delta_{ab} h(q, p) \left( g^{\mu\lambda} - \frac{p^2 q^\mu q^\lambda + q^2 p^\mu p^\lambda - p \cdot q (p^\mu q^\lambda + q^\mu p^\lambda)}{p^2 q^2 - (p \cdot q)^2} \right) , \\ h(q, p) &= imN \left( I(q) + I(p) - 2I(p') + (4m^2 - 2p \cdot q - p'^2)M(p, -q) \right) , \\ -i\Gamma_{\pi, \pi, \rho}^{\mu, abc}(q, p) &= \varepsilon_{abc} \left( q^\mu f(q, p) - p^\mu f(p, q) \right) , \\ f(q, p) &= N \left( -I(q) + p^2 M(p, -q) + 2p \cdot q M_1(q, -p) \right) , \end{aligned} \quad (\text{C.1})$$

with  $p' = -p - q$  and  $N = 4N_c N_f$ .

For the four-meson vertices we only need to consider the special cases needed for the diagrams (b) and (c) in Fig. 3:

$$\begin{aligned}
-i\Gamma_{\sigma,\sigma,\sigma,\sigma}(q,p,-q) &= -N \left\{ \frac{I(p-q) + I(p+q)}{2} + 4m^2 (M(p,q) + M(p,-q)) \right. \\
&\quad \left. + 2(m^2 (4m^2 - p^2 - q^2) - \frac{p^2 q^2}{4}) L(p,-q,p-q) \right\} \\
-i\Gamma_{\sigma,\sigma,\sigma,\sigma}(q,p,-p) &= -N \left\{ I(p+q) + I(0) + 4m^2 (K(p) + K(q) + 2M(p,-q)) \right. \\
&\quad \left. + 2p \cdot q M(p,-q) - q^2 K(q) - p^2 K(p) \right. \\
&\quad \left. + m^2 (16m^2 - 4p^2 - 4q^2 + \frac{p^2 q^2}{m^2}) L(p,-q,0) \right\} \\
-i\Gamma_{\sigma,\pi,\sigma,\pi}^{ab}(q,p,-q) &= \delta_{ab} N \left\{ I(p+q) + I(p-q) + p^2 (4m^2 - q^2) L(p,-q,p-q) \right\} \\
-i\Gamma_{\sigma,\pi,\pi,\sigma}^{ab}(q,p,-p) &= \delta_{ab} N \left\{ -I(p+q) - I(0) - (4m^2 - q^2) (K(q) - p^2 L(p,-q,0)) \right. \\
&\quad \left. + p^2 K(p) - 2p \cdot q M(p,-q) \right\} \\
-i\Gamma_{\pi,\pi,\pi,\pi}^{abcd}(q,p,-q) &= -N \kappa_{abcd} \left\{ I(p+q) + I(p-q) - p^2 q^2 L(p,-q,p-q) \right\} \\
-i\Gamma_{\pi,\pi,\pi,\pi}^{abcd}(q,p,-p) &= -N \kappa_{abcd} \left\{ I(p+q) + I(0) - p^2 K(p) \right. \\
&\quad \left. - q^2 K(q) + 2p \cdot q M(p,-q) + p^2 q^2 L(p,-q,0) \right\} \\
-i\Gamma_{\rho,\sigma,\rho,\sigma}^{ab}(q,p,-q) &= -2\delta_{ab} N \left\{ I(p+q) + I(p-q) + 2I(q) - p \cdot q (M(p,-q) - M(p,q)) \right. \\
&\quad \left. + (4m^2 - 2p^2) (M(p,q) + M(p,-q)) \right. \\
&\quad \left. + m^2 (8m^2 - 6p^2 + 4q^2 + \frac{p^4 - (p \cdot q)^2}{m^2}) L(p,-q,p-q) \right\} \\
-i\Gamma_{\rho,\sigma,\sigma,\rho}^{ab}(q,p,-q) &= -2\delta_{ab} N \left\{ -I(p+q) - I(0) + (p^2 - 4m^2) K(p) \right. \\
&\quad \left. + (q^2 + 2m^2) K(q) + (4m^2 - 2p \cdot q) M(p,-q) \right. \\
&\quad \left. + m^2 (8m^2 - 2p^2 + 4q^2 - \frac{p^2 q^2}{m^2}) L(p,-q,0) \right\} \\
-i\Gamma_{\rho,\pi,\rho,\pi}^{abcd}(q,p,-q) &= 2N \kappa_{abcd} \left\{ -I(p+q) - I(p-q) - 2I(q) \right. \\
&\quad \left. + 2p^2 (M(p,q) + M(p,-q)) + p \cdot q (M(p,-q) - M(p,q)) \right. \\
&\quad \left. + (2m^2 p^2 - p^4 + (p \cdot q)^2) L(p,-q,p-q) \right\} \\
-i\Gamma_{\rho,\pi,\pi,\rho}^{abcd}(q,p,-q) &= 2N \kappa_{abcd} \left\{ I(p+q) + I(0) - p^2 K(p) - (q^2 + 2m^2) K(q) \right. \\
&\quad \left. + 2p \cdot q M(p,-q) + p^2 (2m^2 + q^2) L(p,-q,0) \right\}, \quad (C.2)
\end{aligned}$$

with  $\Gamma_{\rho,M,M,\rho}(q,p,-q) = g_{\mu\nu} \Gamma_{\rho,M,M,\rho}^{\mu\nu}(q,p,-q)$ ,  $\Gamma_{\rho,M,\rho,M}(q,p,-p) = g_{\mu\nu} \Gamma_{\rho,M,\rho,M}^{\mu\nu}(q,p,-p)$  and  $\kappa_{abcd} = \delta_{ab} \delta_{cd} + \delta_{ad} \delta_{bc} - \delta_{ac} \delta_{bd}$ .

## D Expressions at non-zero temperature

To determine the temperature dependence of various quantities we need for the calculation of the quark condensate at non-zero temperature in Sec. 6 we adopt the imaginary time or Matsubara formalism (see e.g. Ref. [42]). In principle this amounts to replace the integration over energy in the zero temperature expressions by a sum over fermionic or bosonic Matsubara frequencies  $\omega_n$ :

$$i \int \frac{d^4 k}{(2\pi)^4} f(k) \rightarrow -T \sum_n \int \frac{d^3 k}{(2\pi)^3} f(i\omega_n, \vec{k}) . \quad (\text{D.1})$$

With this replacement prescription we can define the temperature analogue to the elementary integrals, e.g.

$$\begin{aligned} I(p) &= \int \frac{d^4 k}{(2\pi)^4} \frac{1}{(k^2 - m^2 + i\varepsilon)((k+p)^2 - m^2 + i\varepsilon)} \rightarrow \\ I(i\omega_l, \vec{p}) &= iT \sum_n \int \frac{d^3 k}{(2\pi)^3} \frac{1}{((i\omega_n)^2 - \vec{k}^2 - m^2)((i\omega_n + i\omega_l)^2 - (\vec{k} + \vec{p})^2 - m^2)} \end{aligned} \quad (\text{D.2})$$

This example also illustrates our notation: At non-zero temperature the integral depends on energy and three-momentum separately, which is indicated via a second argument. In that way it can be clearly distinguished from its vacuum counterpart with only one argument. A similar notation is used for other momentum dependent integrals. The non-zero-temperature analogue to the integral  $I_1$  will be denoted by  $I_{1T}$ .

We will now summarize the explicit expressions for various temperature dependent quantities which are related to the determination of the quark condensate at non-zero temperature. The temperature analogue to the gap equation Eq. (B.1) is given by

$$\begin{aligned} m_T &= m_0 - 2g_s 4N_c N_f m_T T \sum_n \int \frac{d^3 k}{(2\pi)^3} \frac{1}{(i\omega_n)^2 - E^2} \\ &= m_0 + 2g_s 4N_c N_f m_T I_{1T} , \end{aligned} \quad (\text{D.3})$$

with  $E = \sqrt{\vec{k}^2 + m_T^2}$  and  $\omega_n = (2n+1)\pi T$  being fermionic Matsubara frequencies.

The polarization functions for the RPA mesons read

$$\begin{aligned} \Pi_\sigma(i\omega_l, \vec{p}) &= 4iN_c N_f I_{1T} - 2iN_c N_f ((i\omega_l)^2 - \vec{p}^2 - 4m_T^2) I(i\omega_l, \vec{p}) \\ \Pi_\pi(i\omega_l, \vec{p}) &= 4iN_c N_f I_{1T} - 2iN_c N_f ((i\omega_l)^2 - \vec{p}^2) I(i\omega_l, \vec{p}) , \end{aligned} \quad (\text{D.4})$$

with  $\omega_l = 2l\pi T$  being bosonic Matsubara frequencies. Below the phase transition the integral  $I_{1T}$  can again be replaced with the help of the gap equation Eq. (D.3) (cf. Eqs. (B.2) to (B.3)).

Finally, the constant  $\Delta_T$  is given by

$$\begin{aligned} \Delta_T &= 4iN_c N_f m_T T \int \frac{d^3 p}{(2\pi)^3} \sum_l \left\{ \right. \\ &\quad D_\sigma(i\omega_l, \vec{p}) (2I(i\omega_l, \vec{p}) + I(0, 0) - ((i\omega_l)^2 - \vec{p}^2 - 4m_T^2) K(i\omega_l, \vec{p})) \\ &\quad \left. + D_\pi(i\omega_l, \vec{p}) (3I(0, 0) - 3((i\omega_l)^2 - \vec{p}^2) K(i\omega_l, \vec{p})) \right\} , \end{aligned} \quad (\text{D.5})$$



where  $\omega_l$  are again bosonic Matsubara frequencies.

## References

- [1] G.E. Brown, Nucl. Phys. A **446**, 12c (1985);  
G.E. Brown, M. Rho and W. Weise, Nucl. Phys. A **454**, 669 (1986).
- [2] M. Herrmann, B. Friman and W. Nörenberg, Nucl. Phys. A **560**, 411 (1993).
- [3] R. Rapp and J. Wambach, preprint hep-ph/9909229, to be published in Adv. Nucl Phys..
- [4] T. Schäfer and E.V. Shuryak, Rev. Mod. Phys. **70**, 323 (1998).
- [5] Y. Nambu and G. Jona-Lasinio, Phys. Rev. **122**, 345 (1961); **124**, 246 (1961).
- [6] U. Vogl and W. Weise, Progr. Part. and Nucl. Phys. **27**, 195 (1991).
- [7] S.P. Klevansky, Rev. Mod. Phys. **64**, 3 (1992).
- [8] T. Hatsuda and T. Kunihiro, Phys. Rep. **247**, 221 (1994).
- [9] S. Klimt, M. Lutz, W. Weise, Phys. Lett. B **249**, 386 (1990).
- [10] M. Lutz, S. Klimt, W. Weise, Nucl. Phys. A **542**, 521 (1992).
- [11] S. Krewald, K. Nakayama and J. Speth, Phys. Lett. B **272**, 190 (1991).
- [12] E. Quack and S.P. Klevansky, Phys. Rev. C **49**, 3283 (1994).
- [13] D. Blaschke, Yu.L. Kalinovsky, G. Röpke, S. Schmidt and M.K. Volkov, Phys. Rev. C **53**, 2394 (1996).
- [14] V. Dmitrašinovič, H.-J. Schulze, R. Tegen and R.H. Lemmer, Ann. Phys. (NY) **238**, 332 (1995).
- [15] E.N. Nikolov, W. Broniowski, C.V. Christov, G. Ripka and K. Goeke, Nucl. Phys. A **608**, 411 (1996).
- [16] R.H. Lemmer and R. Tegen, Nucl. Phys. A **593**, 315 (1995).
- [17] Y.B. He, J. Hüfner, S.P. Klevansky and P. Rehberg, Nucl. Phys. A **630**, 719 (1998).
- [18] M. Huang, P. Zhuang and W. Chao, Phys. Lett. B **465**, 55 (1999); preprint hep-ph/9903304.
- [19] M. Oertel, M. Buballa and J. Wambach, Phys. Lett. B **477**, 77 (2000).
- [20] M. Oertel, M. Buballa and J. Wambach, Nucl. Phys. A **676**, 247 (2000).
- [21] R.S. Plant and M.C. Birse, preprint hep-ph/0007340.

- [22] H. Kleinert and B. Van den Bossche, Phys. Lett B **474**, 336 (2000); hep-ph/9908284.
- [23] W. Florkowski, W. Broniowski, Phys. Lett. B **386**, 62 (1996).
- [24] S. Klimt, M. Lutz, U. Vogl and W. Weise, Nucl. Phys. A **516**, 429 (1990).
- [25] L.M. Luttinger and J.C. Ward, Phys. Rev. **118**, 1417 (1960).
- [26] G. Baym and L.P. Kadanoff, Phys. Rev. **124**, 287 (1961); G. Baym, Phys. Rev. **127**, 1391 (1962).
- [27] G. Ripka, *Quarks bound by chiral fields*, Clarendon Press, Oxford 1997.
- [28] E. Babaev, preprint hep-ph/0006087, to be published in Phys. Rev. D.
- [29] P. Nozieres and S. Schmitt-Rink, J. Low Temp. Phys. **59**, 195 (1985).
- [30] C.A.R. Sá de Melo, M. Randeria and J.R. Engelbrecht, Phys. Rev. Lett. **71**, 3202 (1993).
- [31] G. Ripka, preprints hep-ph/0003201; hep-ph/0007250.
- [32] H.G. Dosch and S. Narison, Phys. Lett. B **417**, 173 (1998).
- [33] L. Giusti, F. Rapuano, M. Talevi and A. Vladikas, Nucl. Phys. B **538**, 249 (1999).
- [34] M. Lutz and W. Weise, Nucl. Phys. A **518**, 156 (1990).
- [35] L.M. Barkov et al., Nucl. Phys. B **256**, 365 (1985); S.R. Amendolia et al., Phys. Lett. B **138**, 454 (1984).
- [36] C.D. Frogatt, J.L. Petersen, Nucl. Phys. B **129**, 89 (1977).
- [37] S.R. Amendolia et al., Nucl. Phys. B **277**, 168 (1986).
- [38] R.K. Bhaduri, *Models of the Nucleon*, Addison-Wesley, Redwood City, California 1988.
- [39] D. Davesne, Y.J. Zhang and G. Chanfray, preprint nucl-th/9909032.
- [40] V. Bernard, U.-G. Meißner, A.H. Blin, B. Hiller, Phys. Lett. B **253**, 443 (1991).
- [41] J. Gasser, H. Leutwyler, Phys. Lett. B **184**, 83 (1987); Phys. Lett. B **188**, 477 (1987); Nucl. Phys. B **307**, 763 (1988).
- [42] A.L. Fetter , J.D. Walecka, *Quantum Theory of Many-Particle Systems*, McGraw-Hill, New York 1971.
- [43] F. Karsch and E. Laermann, Phys. Rev. D **50**, 6954 (1994); S. Digal, E. Laermann and H. Satz, preprint hep-ph/0007175.
- [44] R.D. Pisarski and F. Wilczek, Phys. Rev. D **29**, 338 (1984).

- [45] A. Kocić and J. Kogut, Phys. Rev. Lett **75**, 3109 (1995); Nucl. Phys. B **455**, 229 (1995).
- [46] G. Passarino, M. Veltman, Nucl. Phys. B **160**, 151 (1979).
- [47] G.J. van Oldenborgh, J.A.M. Vermaseren, Z. Phys. C **46**, 425 (1990).
- [48] G. 't Hooft, M. Veltman, Nucl. Phys. B **153**, 365 (1979).
- [49] C. Itzykson and J.-B. Zuber, *Quantum Field Theory*, McGraw-Hill, New York 1980.